8-2016

Fluorochlorozirconate Glass Ceramics for Computed Radiography

Adam Wesley Evans
University of Tennessee, Knoxville, aevans27@vols.utk.edu

To the Graduate Council:

I am submitting herewith a thesis written by Adam Wesley Evans entitled "Fluorochlorozirconate Glass Ceramics for Computed Radiography." I have examined the final electronic copy of this thesis for form and content and recommend that it be accepted in partial fulfillment of the requirements for the degree of Master of Science, with a major in Biomedical Engineering.

Jacqueline A. Johnson, Major Professor

We have read this thesis and recommend its acceptance:

Andy Sarles, Jens Gregor

Accepted for the Council:
Carolyn R. Hodges

Vice Provost and Dean of the Graduate School

(Original signatures are on file with official student records.)

Fluorochlorozirconate Glass Ceramics for Computed Radiography

A Thesis Presented for the
Master of Science
Degree
The University of Tennessee, Knoxville

Adam Wesley Evans
August 2016

This thesis is dedicated to my family and childhood friends. Without their guidance and support, I would not be the man I am today.

ACKNOWLEDGEMENTS

I would like to express my sincere appreciation for my advisor, Dr. Jacqueline Johnson, having the confidence to bring me to The University of Tennessee Space Institute. Without her generosity and support, this thesis would not exist.

I would also like to thank Dr. Andy Sarles and Dr. Jens Gregor for their participation in my Thesis Committee.

Several people contributed to this research whom I wish to thank. Kathleen Lansford, Alexander Terekhov, and Doug Warnberg provided technical assistance. Dr. Lloyd Arrowood and Alex Moses for performing sample exposures, and Dr. Richard Lubinsky (SUNY Stony Brook) for performing the photostimulated luminescence light output measurements.

I have enjoyed my time at UTSI. Jason Hah, Phillip Clarke, Stu Steen, Brett Shields, JavadSeif, Matt Dimaiolo, Kris Oegema, and Dave Surmick have been great friends. The scenery is beautiful, and my Magic: the Gathering friends in the Tullahoma area have provided a welcome distraction from my studies when needed.

In particular, I want to give special thanks to my fellow groupmates Dr. Lee Leonard and Julie King. I am grateful for Lee, his training and knowledge in the lab, company at the GOMD 2016 conference, input on numerous presentations and experiments, and his help with the creation of the radiographic images used in this thesis. I am especially grateful for Julie, who took me under her wing when I arrived and showed me how to be a graduate student.

ABSTRACT

Heat treating fluorochlorozirconate (FCZ) glasses precipitates nanocrystals in the glass matrix, resulting in a glass ceramic that has optical properties suitable for use as a medical imaging plate. As the temperature of heat treatment rises, the resulting FCZ glass-ceramic becomes increasingly more opaque as the size of the orthorhombic phase $BaCl_2$[barium chloride] nanocrystals grow within the glass matrix. This opaqueness negatively affects imaging. The effect of adding Fe^{3+}[iron] on the valence state of zirconium and overall glass quality was investigated.

Samples were synthesized and characterized with differential scanning calorimetry to determine the temperature of the orthorhombic $BaCl_2$[barium chloride] phase transition. Samples were then heat treated to create a glass ceramic with the desired storage phosphor properties. Phosphorimetry and x-ray diffraction (XRD) experiments were performed on the glass ceramics to confirm crystal phases. Finally, photostimulated luminescence (PSL) experiments were performed to measure light output. Results showed that the addition of small amounts of $FeCl_3$[iron chloride] (1-2%) to a ZBLAN glass composition allows for the precipitation of orthorhombic phase $BaCl_2$[barium chloride] crystals while maintaining transparency of the glass-ceramic.

Additionally, larger FCZ plates were synthesized and heat treated for performance testing as a storage phosphor image plate. Plates were exposed at various x-ray energies (45 keV - 1 MeV) and used to image numerous phantoms and everyday items. The suitability of fluorochlorozirconate glass as a storage phosphor imaging plate for computed radiography was evaluated.

TABLE OF CONTENTS

LIST OF TABLES

LIST OF FIGURES

CHAPTER 1:
INTRODUCTION & GENERAL INFORMATION

Fluorochlorozirconate Glass / Glass Ceramics

Fluorozirconate (FZ) glasses have undergone continual development since their initial discovery in 1975. Originally containing 50% ZrF_4, 25% BaF_2, and 25% NaF [1], the FZ composition was systematically modified in an attempt to achieve specific glass properties. These modifications lead to the FZ glass system known as ZBLAN (ZF_4-BaF_2-LaF_3-AlF_3-NaF). The addition of AlF_3 and LaF_3 resulted in a more stable glass [2-5].

With its high chemical stability and ability to host rare earth dopants, ZBLAN has been used in fields from optical fibers to photovoltaics [6]. A modified ZBLAN composition, known as a fluorochlorozirconate glass, was pursued as a possible improvement over current storage phosphor plate technology [7-14] due its low phonon energy [15-19] that reduces non-radiative energy losses.

Fluorochlorozirconate (FCZ) glass is a modified ZBLAN composition in which chlorine is added to the matrix through substitutions such as $BaCl_2$ for BaF_2 or NaCl for NaF. The addition of chlorine allows for the nucleation of phase specific $BaCl_2$ nanocrystals within the glass matrix during heat treatment. [20].The synthesized glass becomes a glass-ceramic after heat treatment.

The properties of the glass-ceramic can be changed by tuning the phase of $BaCl_2$ nanocrystals within the glass matrix during heat treatment. The phase transformation of $BaCl_2$ has a significant effect on the optical properties of the resultant glass-ceramic: hexagonal phase $BaCl_2$ scintillates (converts ionizing radiation to visible light), while orthorhombic phase $BaCl_2$ exhibits storage characteristics when irradiated with x-rays (converts radiation into stable electron-hole pairs for later readout with a laser beam) [7-9].This difference is shown further in Figure 1. FCZ scintillators have uses in indirect digital radiography (DR) and computed tomography systems for medical applications. FCZ storage phosphors, on the other hand, are employed as a reusable imaging plate for x-ray medical imaging in a technique known as computed radiography (CR).

FCZ glass-ceramics containing orthorhombic $BaCl_2:Eu^{2+}$ nanocrystals have shown the potential for greatly improved resolution when compared to traditional storage phosphor materials [21, 22]. With crystals much smaller in diameter (50-100 nm) than the wavelength of the stimulating light, scattering is greatly reduced

and resolution is improved [7, 23, 24]. For these reasons, FCZ glass-ceramics are an attractive option to replace current x-ray storage phosphor technology (BaBrF:Eu) [12, 25,26].

FCZ glasses, however, do encounter some complications during production. Zirconium fluoride is a volatile compound above 450 ºC in ZrF_4-based glasses [27]. ZBLAN glasses experience losses of ~15% during the high temperature of the synthesis process. Some of this weight loss is attributed to the sublimation of ZrF_4 during synthesis. The greater loss of anions causes a portion of the remaining ZrF_4 in the glass matrix to reduce to ZrF_3, contributing to the formation of black spots throughout the newly synthesized glass [27].These black spots are less than ideal for artifact free images and/or high spatial resolution.

In order to help stabilize the valence state of zirconium within the glass matrix, small amounts (0-4%) of $FeCl_3$were added to the glass composition. Iron can exist in many oxidation states, most commonly as Fe^{2+} and Fe^{3+}. The author hypothesized that the versatility of the iron valence state will help stabilize zirconium from reducing during synthesis, resulting in a final product with better optical properties and light output overall. This is the first time iron chloride has been added to a ZBLAN composition to improve its quality for imaging applications.

Computed Radiography

Computed radiography (CR) is an imaging modality currently being used in medicine. The numbers of screen film (SF) radiography systems are on the decline as they are being replaced by CR and digital radiography (DR) systems. These systems differ in detection medium and image storage. Traditional screen film radiography systems store the image on a film during x-ray radiation. The image is developed later in a chemical process. In computed radiography, the image is made through the creation of electron hole pair traps in the photostimulable storage phosphor plate while the plate is exposed to x-ray radiation. Once the image is stored in the plate, it can be read through laser stimulation of the plate that causes the hole pairs to recombine, releasing photons that can be converted into a digital image. Indirect digital radiography uses a flat panel display with a scintillator material that luminesces under x-ray radiation. Light is converted to electrical charge that can be used to create a digital image.

Each system has its advantages and disadvantages. The digital images of both DR and CR systems allow for image processing and software to produce a higher quality final image. This also reduces the amount of retakes that must be done, limiting patient x-ray dose. These digital images are able to be quickly

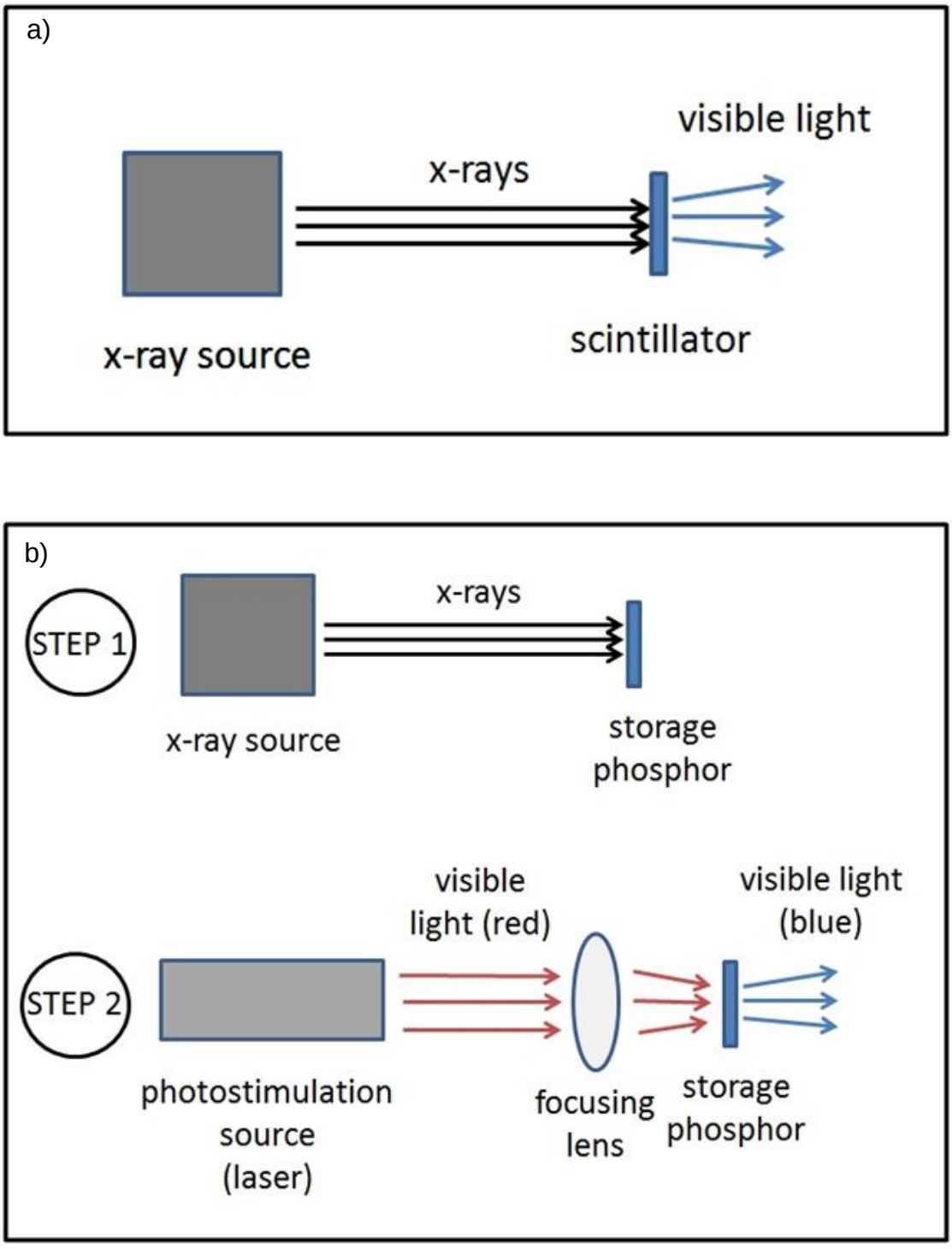

Figure 1. Difference in visible light emission for a) scintillators versus b) storage phosphors. Credit: Russell Lee Leonard, UTSI. Used with permission.

transferred to other locations and stored electronically. Screen film produces a physical copy that takes up storage space and is more cumbersome to transfer. CR and DR eliminate darkroom problems associated with odor and chemical hazards. The storage phosphor imaging plates of CR are able to be reused, reducing film costs overall. While DR is the fastest modality at producing images, its equipment cost is also the most expensive.

Computed Radiography Imaging Plates

Computed radiography imaging systems use plates synthesized from photostimulable luminescent materials. The plate is encased in a cassette opaque to visible light but transparent to x-ray radiation. After a CR imaging plate has been exposed to radiation, it is transported to a dark room for readout. The plate is removed from the cassette and placed on the scanner. The scanner's laser beam passes over the plate pixel by pixel, causing the trapped electron hole pairs to recombine and emit light that is collected in a photomultiplier tube (PMT); light from the stimulating laser is removed by a filter before reaching the PMT. This signal is converted into the digital image. Once the image has been created, the plate can be erased through exposure to light of appropriate wavelength and sufficient intensity, then returned to its casing for subsequent exposures. This process is shown in Figure 2.

Commercial CR plates currently consist of storage phosphor crystallites in a binder between a layer of backing material and a protective outer coating. X-ray radiation causes electron hole pairs to become trapped within the defects of the material. The latent image is stored as these trapped hole pairs. Laser stimulation provides the hole pair with enough energy to recombine, releasing a characteristic photon. This process of stimulation, storage, and readout has been termed photostimulated luminescence [28].

Commercial CR experiences lower resolution due to scattering of the laser beam during readout [29]. This occurs when the stimulating laser interacts with the storage phosphor crystallites within the binder material. A schematic of this issue is shown in Figure 3. Scattering causes inaccuracies; the laser stimulates at one pixel during readout and may scatter upon striking a storage phosphor crystallite in the binder material, causing absorption and emission at an adjacent pixel. The emission from the adjacent pixel is collected by the scanner but is recorded by the computer as being from the original pixel, causing inaccuracies in the final image.

As mentioned before, FCZ glass-ceramics containing orthorhombic $BaCl_2:Eu^{2+}$ nanocrystals have shown the potential for greatly improved resolution when compared to traditional storage phosphor materials. With nanocrystals much

smaller in diameter (50-100 nm) than the wavelength of the stimulating light, scattering is greatly reduced and resolution is improved.

In this work, FCZ storage phosphors plates were synthesized and tested at various x-ray energies (45 keV-1 MeV) to determine their potential in computed radiography applications.

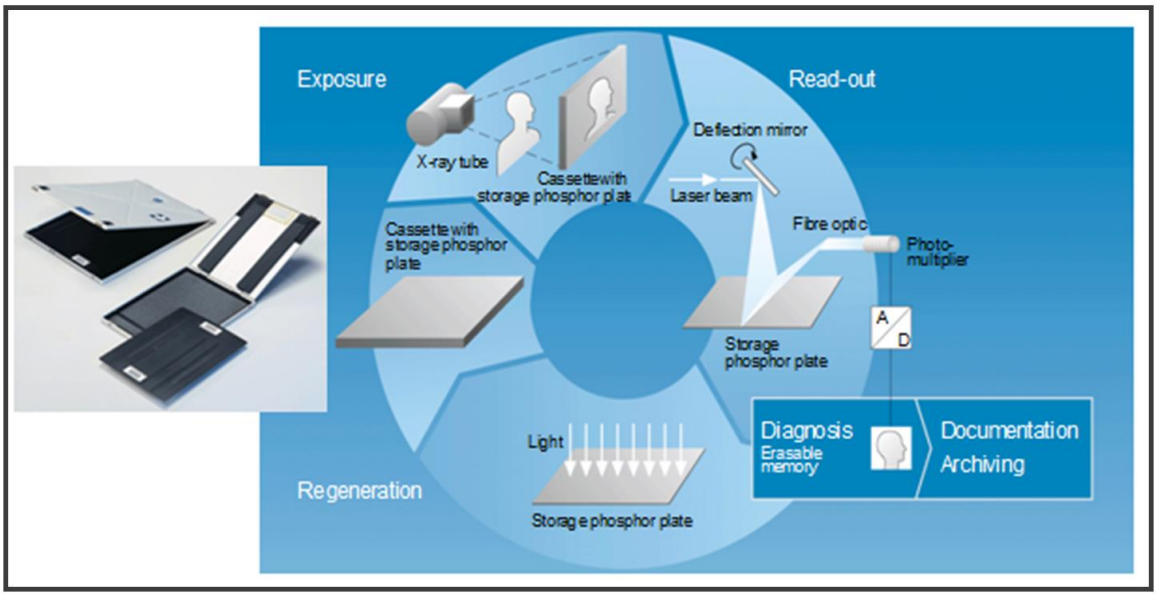

Figure 2. Computed radiography imaging cycle.

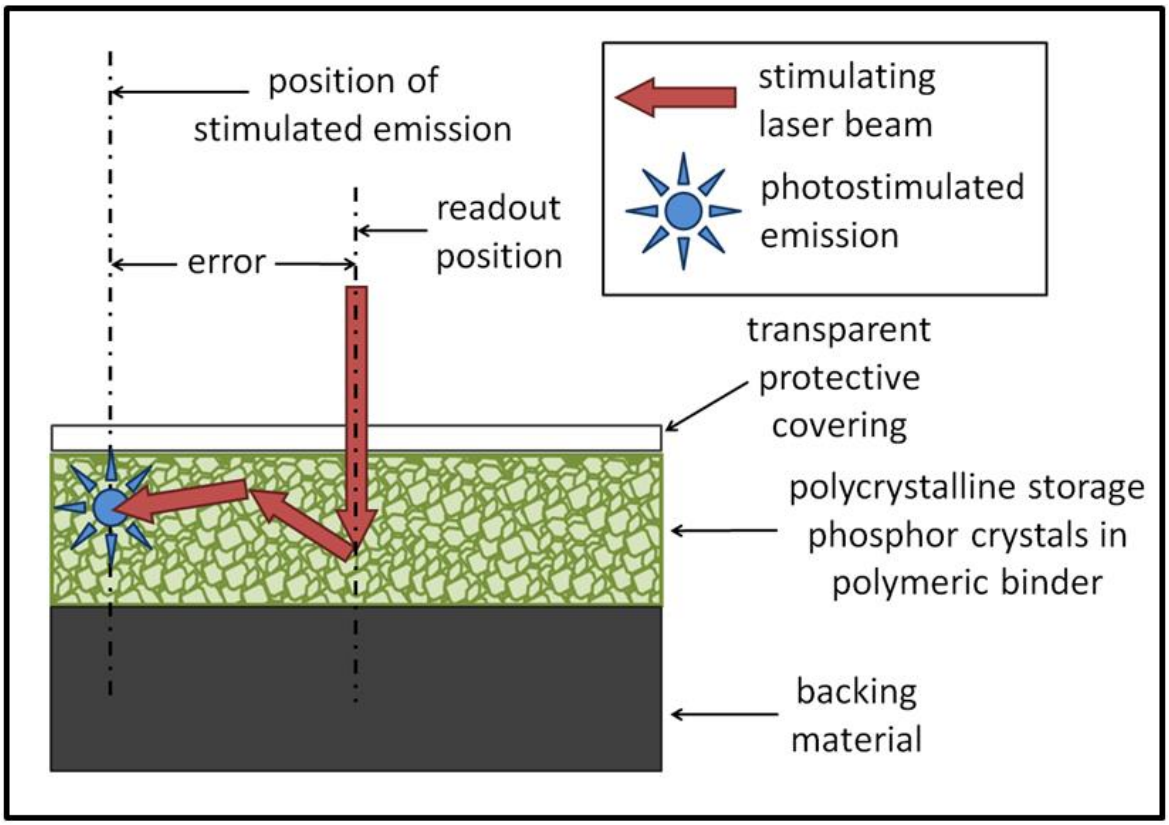

Figure 3. Difficulties in imaging with polycrystalline storage phosphor materials [30]. Used with permission.

CHAPTER 2:

MATERIALS & METHODS

Sample Preparation

All samples were produced in an MBraun LABmaster SP glovebox with an adjacent OTF-1200-2 dual zone tube furnace (MTI Corporation). Both the glovebox and furnace contain argon gas to provide an inert atmosphere during synthesis. Oxygen and moisture contamination were monitored and consistently remained below 0.1 ppm. Furnace temperature during the melting process was measured using a thermocouple inside the ceramic tube of the furnace for accurate readout. Argon gas was continuously purged through the furnace during synthesis to limit contamination. Precursor chemicals were anhydrous and stored and opened in the glovebox to minimize contamination. An image of the system is shown in Figure 4.

Glass Synthesis

For investigation into $FeCl_3$ doping, ten total glass samples were produced. These ten samples were divided into two groups of five based on optically active rare earths ($EuCl_2$ or $EuCl_3$). The amount of iron chloride was increased from 0% to 4% in whole number increments. Table 1 shows the composition of each $FeCl_3$ sample doped with $EuCl_2$, while Table 2 shows the composition of $FeCl_3$ samples doped with $EuCl_3$. The weight of each sample's constituents was ten grams before furnace melt.

Samples were produced in a two-step process to help decrease evaporation of chlorides during the high temperature melting stage. In the first step, fluoride compounds were weighed, mixed in a platinum crucible, covered with a platinum lid, and heated in the adjacent furnace according to the heating profile shown in Figure 5. The fluoride mixture was dried at 400 ºC for sixty minutes before ramping to 800 ºC and holding for another sixty minutes. At this point, the fluoride mixture was removed from the furnace and allowed to cool to room temperature in the glovebox. Once cool, the chlorides were weighed and added to the existing fluoride mixture, then returned to the furnace at 750 ºC. The glass mixture was heated at this temperature for sixty minutes, ramped down to 700 ºC for five minutes, and idled at 700 ºC for another five minutes. The temperature is decreased in the final ten minutes to fine the glass, reducing the size and amount of bubbles in the final poured sample.

When heating is complete, the sample was removed from the furnace and poured into a 200 ºC brass mold to cool. The cartridge heaters in the brass mold

were programmed to return to room temperature over the course of four hours. Temperature of the mold was monitored with a thermocouple and controlled with a proportional-integral-derivative (PID) controller. Figure 6 shows an example of a glass being poured into the preheated glass mold. The 200 ºC temperature for the preheated mold was chosen because it is below the crystallization temperature of the glass. The rapid cooling of the glass from the 700 ºC pour to the 200 ºC mold prevents devitrification.

Once cooled, the glass sample is removed from the mold and cut into smaller pieces (1 cm^2) for characterization. Figure 7 shows a typical sample already removed from the mold. Samples were stored in a desiccator when not being studied to suppress atmospheric contamination.

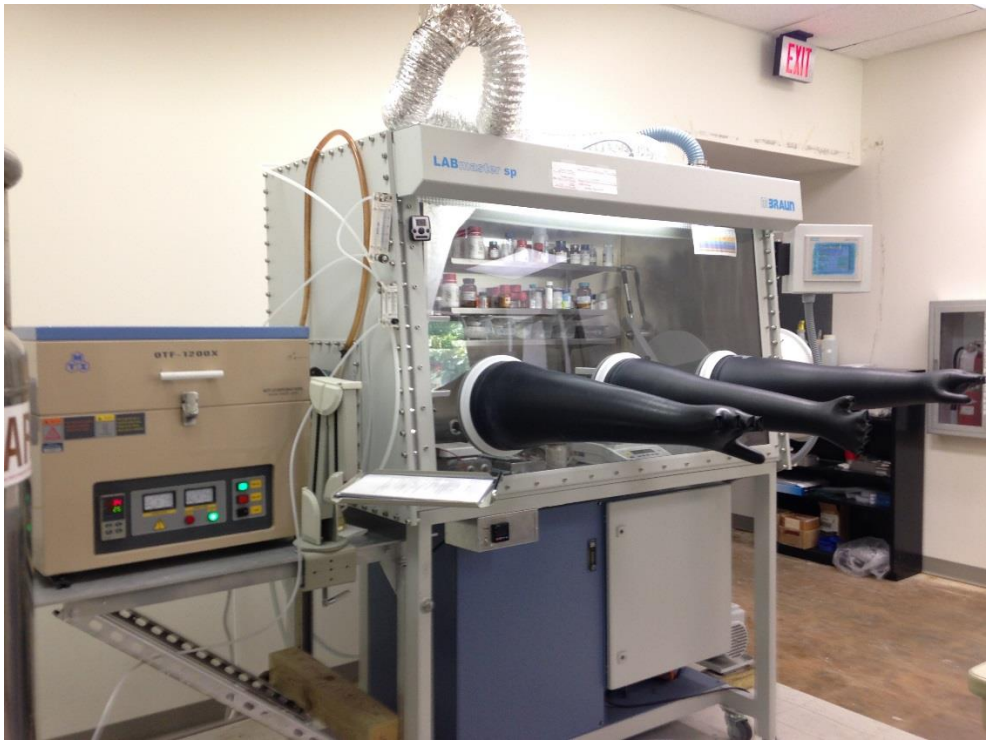

Figure 4.Glovebox and adjacent tube furnace for sample production

Table 1. Compositions of samples doped with $EuCl_2$ in mole percent

Sample	ZrF_4	$BaCl_2$	NaF	AlF_3	LaF_3	InF_3	$EuCl_2$	$EuCl_3$	$FeCl_3$
JJ162	51	20	20	3	3.5	0.5	2	0	0
JJ172	51	19	20	3	3.5	0.5	2	0	1
JJ165	51	18	20	3	3.5	0.5	2	0	2
JJ170	51	17	20	3	3.5	0.5	2	0	3
JJ167	51	16	20	3	3.5	0.5	2	0	4

Table 2. Compositions of samples doped with $EuCl_3$ in mole percent

Sample	ZrF_4	$BaCl_2$	NaF	AlF_3	LaF_3	InF_3	$EuCl_2$	$EuCl_3$	$FeCl_3$
JJ161	51	20	20	3	3.5	0.5	0	2	0
JJ171	51	19	20	3	3.5	0.5	0	2	1
JJ164	51	18	20	3	3.5	0.5	0	2	2
JJ169	51	17	20	3	3.5	0.5	0	2	3
JJ166	51	16	20	3	3.5	0.5	0	2	4

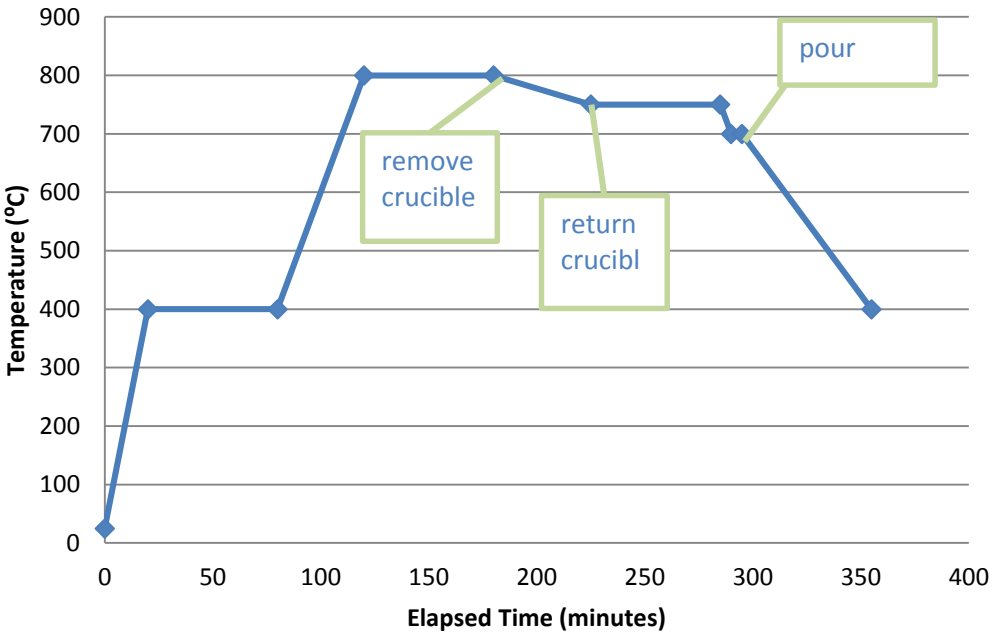

Figure 5. Heating profile for two-step melt synthesis

Figure 6. Molten FCZ glass being poured into preheated brass mold.

Figure 7. Example of synthesized amorphous glass sample once removed from mold. A quarter is shown for scale.

Synthesis of glass plates for computed radiography followed a different heating method. Table 3 shows the composition of each plate sample. The weight of the sample's constituents varied between thirty and forty grams before furnace melt. A larger amount of precursor chemicals results a larger final glass plate. Contrary to the $FeCl_3$ samples, plate samples were produced in a newly developed one step process. Before mixing all compounds together, ZrF_4 and $BaCl_2$ were individually dried in the adjacent tube furnace at 300 ºC for ten minutes. These chemicals were chosen to be dried because they are the most hygroscopic of the precursor materials, and water can result in negative outcomes for the resultant glass.

After individually drying ZrF_4 and $BaCl_2$, all compounds were weighed, mixed in a platinum crucible, covered with a platinum lid, and heated in the adjacent furnace. The mixture dried at 300 ºC for twenty minutes before ramping to 825 ºC and holding for another thirty minutes. The glass mixture then ramped down to 775 ºC for five minutes, and idled at 775 ºC for another five minutes. The temperature is decreased in the final ten minutes to fine the glass and reduce bubbles in the final poured sample.

Once heating was complete, these samples underwent the same cooling, processing, and storage procedures as the $FeCl_3$ doped samples.

Table 3. Compositions of larger plate samples in mole percent

Sample	ZrF_4	$BaCl_2$	NaF	AlF_3	LaF_3	InF_3	$EuCl_2$
ZBLAN30	44.21	22.71	23.11	2.60	3.03	1.73	2.60
ZBLAN40	47.82	19.88	25	2.81	3.28	0.47	0.75

Glass Ceramic Synthesis

As-made glass samples were heat treated in order to precipitate a desired crystalline phase of $BaCl_2$ (orthorhombic) within the FCZ glass matrix. The temperatures of heat treatment for each sample were determined by differential scanning calorimetry analysis detailed in the characterization section.

$FeCl_3$ samples were heat treated using a two-step process. 1 cm^2 portions of glass were placed on a brass sheet and preheated to below the glass transition temperature (typically 210 ºC). This operation was done to help prevent thermal shock in the glass. Once preheated, the sample was transferred to a preheated covered aluminum boat with embedded thermocouple and placed inside an Electro Application Inc. tube furnace at the desired temperature. An image of this system is shown in Figure 8. Temperatures were monitored and recorded

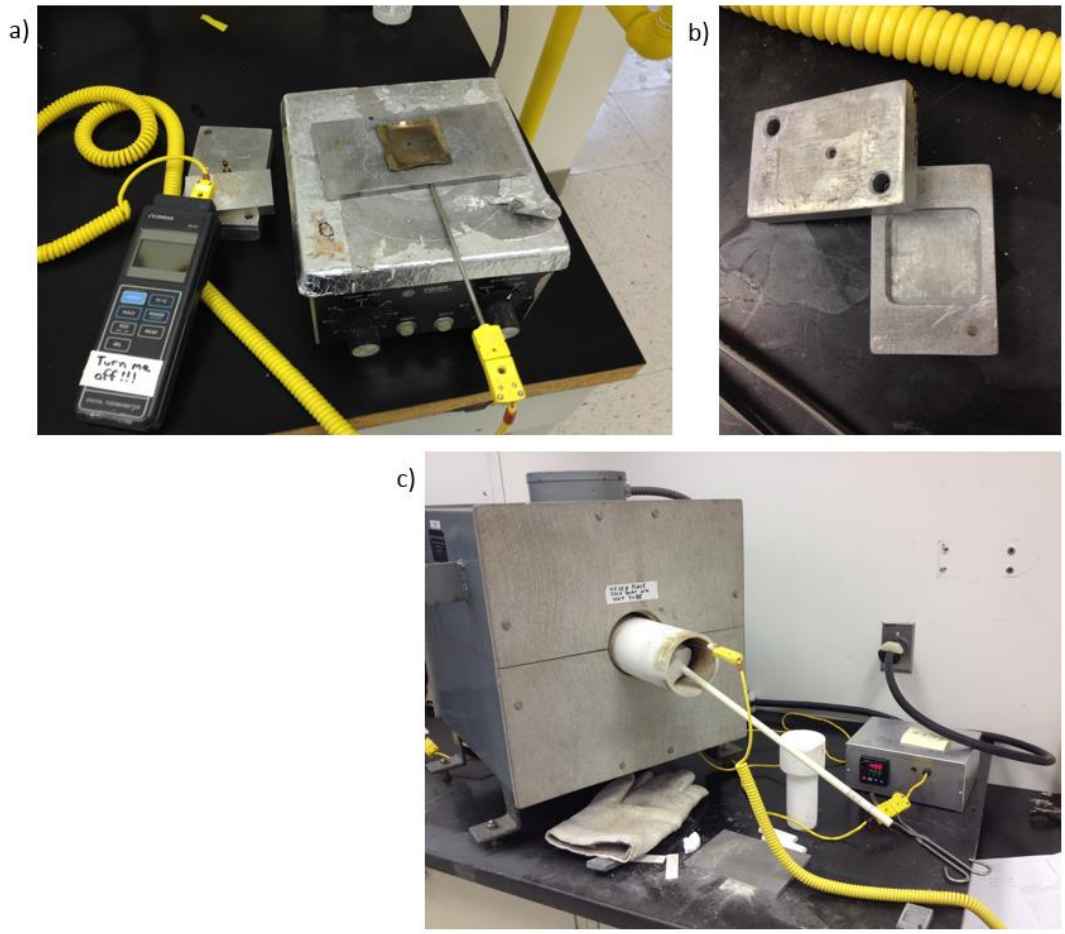

Figure 8. Setup for glass ceramic heat treatment. a) Brass sheet for preheating to below the glass transition temperature. b) Aluminum boat for holding sample and thermocouple in the furnace. c) Electro Application Inc. tube furnace with inserted sample and thermocouple.

throughout heat treatment at one minute intervals. After five minutes at the desired temperature, the boat was removed and placed on a 200 ºC hot plate, then allowed to slowly cool to room temperature, again to avoid thermal shock.

FCZ plates were heat treated using a newer one-step process. 1 cm^2 portions of glass were placed inside a split aluminum block at room temperature. Each half of the aluminum block has its own set of thermocouples and cartridge heaters. Cartridge heaters were controlled with proportional-integral-derivative (PID) controllers, allowing for consistent heating rates. Figure 9 shows this system. The sample was subjected to a programmed heating cycle. The room temperature glass sample was heated to 200 ºC, held for five minutes, and then ramped to the desired temperature at a rate of five degrees per minute. Once at the desired temperature, the sample was held for five minutes, and then cooled to room temperature at a rate of five degrees per minute. The fan (pictured in Figure 9) provided cooling by convection; the cartridge heaters prevented uncontrolled cooling.

Once heat treated, the glass ceramic samples luminesce when exposed to UV light. The color of the emission can be a quick indicator as to whether the desired phase of $BaCl_2$ was precipitated in the glass matrix. Blue luminescence indicates the presence of hexagonal phase nanocrystals and violet luminescence indicates the presence of orthorhombic phase $BaCl_2$ nanocrystals within the FCZ glass matrix. An example of this color change can be seen in Figure 10, where the samples were photographed while exposed to 254 nm light.

Figure 9. Newer heat treatment system with split aluminum block and separate cartridge heaters and PID controllers

Figure 10. An example of color change post heat treatment. Samples are exposed to 254 nm black light. Blue/cyan corresponds to hexagonal phase $BaCl_2$ nanocrystals, while violet corresponds to orthorhombic phase $BaCl_2:Eu^{2+}$ nanocrystals within the FCZ glass matrix.

Characterization

1. Differential Scanning Calorimetry (DSC)

Differential Scanning Calorimetry (DSC) was used to determine the glass transition temperature (T_g) and crystallization temperature of the samples. A Netzsch DSC 200F3 (NETZSCH) was used for measurements, and analysis was done with Netzsch Proteus Thermal Analysis Software (Version 5.2.1) to determine phase transformation temperatures.

Aliquots were taken from the interior of each sample. These fragments weighed 20 ± 10 mg. Each aliquot was placed in a Netzch Aluminum 25 µL crucible and sealed with an aluminum lid. The sample was placed in the DSC chamber as shown in Figure 11. The left sensor is for the test sample and the right sensor is for an empty reference crucible. During the heating process, the chamber was purged with nitrogen at a rate of 40 mL/min. The samples were heated from 100 ºC to 400 ºC at a rate of either 1 ºC or 10 ºC per minute.

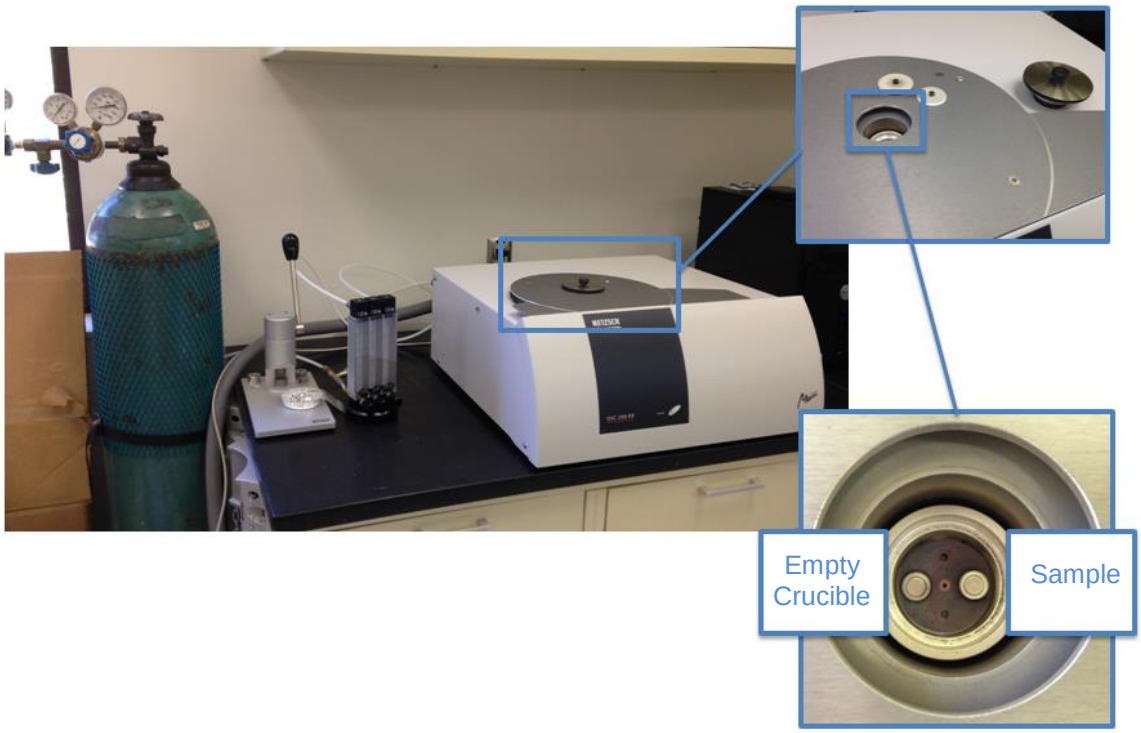

Figure 11. Netzsch DSC 200F3 Differential Scanning Calorimeter used for DSC analysis

2. Phosphorimetry

Phosphorimetry was performed on each of the heat treated samples to determine the crystalline phases of $BaCl_2$ within the sample. Gated and emission spectra were acquired using a PTI QM30 model 810/840 Phosphorescence / Fluorescence Spectrofluorometer (Birmingham, NJ). PTI Felix32 software was used to analyze the data. A gated excitation scan excites a sample within a given range of wavelengths and measures the amount of emission at a specific wavelength. A gated emission scan excites the sample at a specific wavelength and measures the amount of emission over a range of wavelengths. An image of the system is shown in Figure 12. Measurements are taken in a darkened room to avoid light contamination. The employed excitation and emission scans used for each glass ceramic are shown in Table 4.

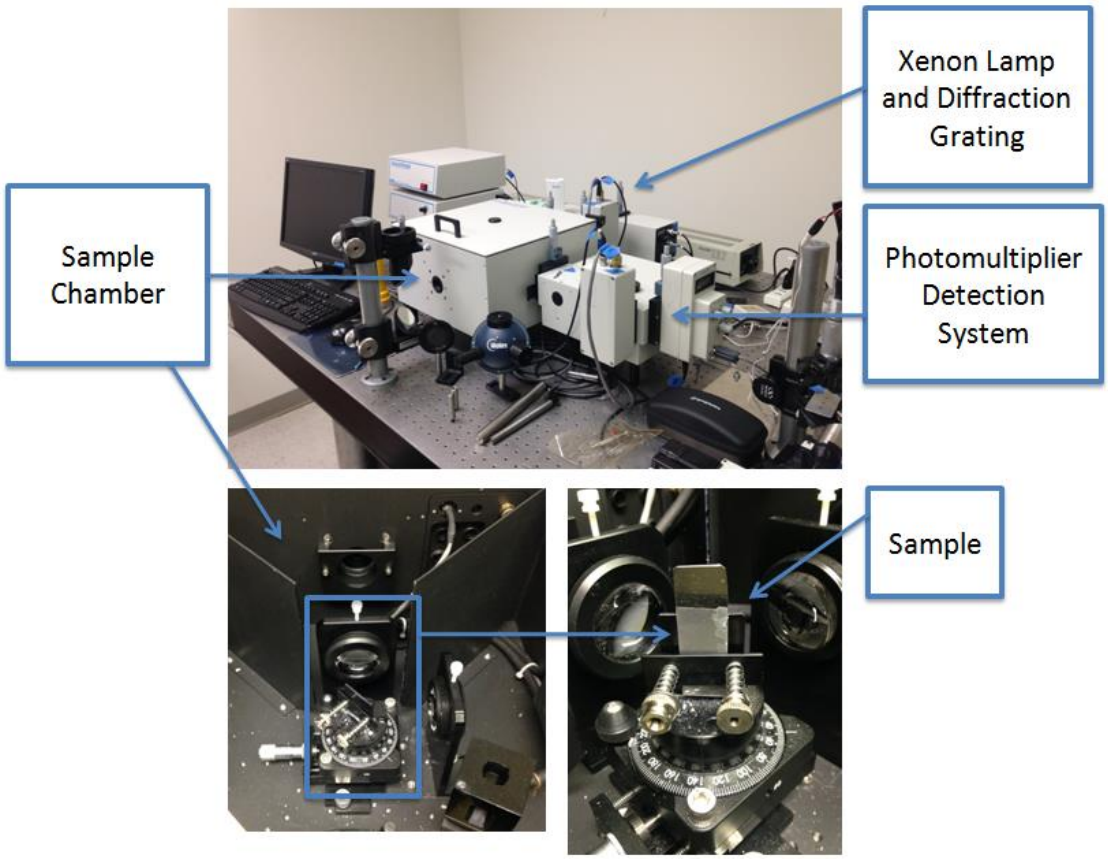

Figure 12. Configuration of the PTI QM30 model 810/840 Phosphorescence / Fluorescence Spectrofluorometer used to acquire PL measurements.

Table 4. Gated excitation and emission scans performed on glass ceramic samples.

Gated Excitation Scans		Gated Emission Scans	
Wavelength Range (nm)	Emission Wavelength (nm)	Excitation Wavelength (nm)	Wavelength Range (nm)
225-400	410	270	280-600
225-460	470	360	370-600

3. *X-Ray Diffraction (XRD)*

X-ray diffraction (XRD) was used to identify and confirm crystal phases within the glass ceramic samples. After heat treatment, the glass ceramic sample is polished to expose the bulk. Characterization was performed using a Philips X'Pert XRD with Cu Kα radiation (λ = 1.54 Å). The machine is shown in Figure 13. Samples were attached to an aluminum peg on the XRD stage with double-sided tape. Measurements were taken over a 2θ range from 20º to 80º at a rate of 0.25 degrees per minute. MDI Jade 9 software was used for data analysis and determination of crystal phases. Characteristic diffraction patterns were compared to diffraction pattern files in the Jade software.

Figure 13. Philips X'Pert XRD used for x-ray diffraction measurements.

4. *Photostimulated Luminescence (PSL)*

Photostimulated Luminescence experiments were performed by Dr. Richard Lubinsky at SUNY Stony Brook in Stony Brook, NY. Integrated PSL signal, or total light output, was measured for each of the heat-treated glass ceramics. Glass ceramic samples were exposed with 70 keV x-rays for 2.5 seconds, totaling an eight Roentgen dose.

Scanner Setup

The scanner apparatus was set up to take computed radiography images in accordance with “Scanning translucent glass-ceramic x-ray storage phosphors" by Lubinsky et al. [31]. A picture of the apparatus can be seen in Figure 14.

After a glass ceramic imaging plate has been exposed to radiation, the plate was placed on a translating stage in the scanner. As the sample moved forward on the floor at constant rate, the solid-state stimulating laser scanned horizontally across the sample from above. The scanner features a telecentric lens system that allows for the incident stimulating laser to always be perpendicular to the plate while scanning. This limits inaccuracies in the image upon readout. Once stimulated, emitted light passes through a band pass filter that removes the stimulating light while allowing the PSL signal to pass through. The light is collected in a photomultiplier tube and the signal passes through a pre-amplifier to a data acquisition card. The radiographic image is constructed on a personal computer using a MATLAB program.

Imaging Plate Exposure

Plates were exposed to x-ray radiation with a Varian Linear Accelerator. Exposures were done at 70 keV, 300 keV, 1 MeV, and 9 MeV. Dose varied from 630 to 20000 Roentgens. Focal spot of the beam was 1.2 millimeters and plates were exposed for times ranging from six minutes to thirty-four minutes. These parameters varied based on the application being tested. At a later time, samples were exposed at 45 keV with a Philips X’Pert XRD with Cu Kα radiation ($\lambda = 1.54$ Å).

Samples were exposed in conjunction with line-pair phantoms, edge phantoms, weld phantoms, and gap phantoms. Conventional everyday items, such as a socket-head cap screw and European hornet were also imaged. Line-pair phantoms feature alternating dark and light vertical lines that act as a measure of spatial resolution. As the line-pairs become more compressed, it is more difficult for an imaging system to resolve them. An example of a line-pair phantom can be seen in Figure 15. Edge phantoms provide a solid break between attenuated and not attenuated regions of the imaging plate. The sharpness of this break, or “edge,” can be measured and processed in a program such as ImageJ to calculate the modulation transfer function (MTF), another measure of spatial frequency. Weld phantoms feature a weld with a known defect. The goal of the weld phantom is to detect this known defect with the imaging plate and scanner. Finally, gap phantoms feature voids, or “gaps,” within a material of various known thicknesses. Much like the weld phantom, the goal with a gap phantom is to detect the difference in thicknesses amongst the gaps.

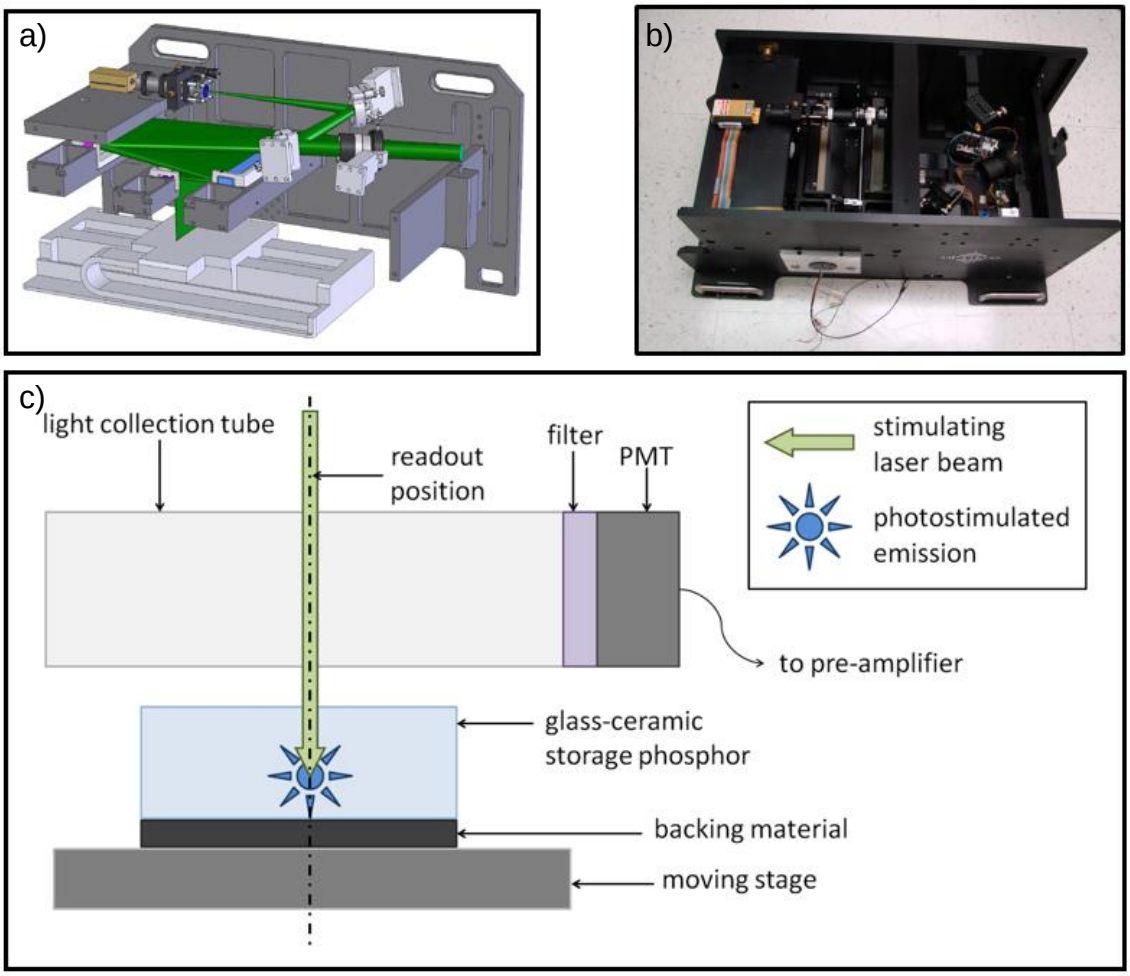

Figure 14. a) CAD rendering of scanner [31], b) photograph of scanner with lid removed (ancillary equipment not shown), and c) simplified cross section of system during readout. Used with permission.

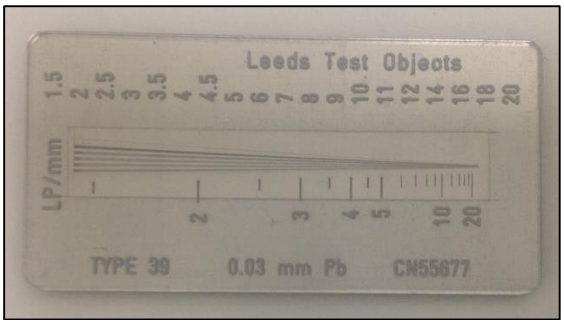

Figure 15. Example of a line pair phantom.

CHAPTER 3:
RESULTS & DISCUSSION

$FeCl_3$ Samples

5. Differential Scanning Calorimetry (DSC)

DSC scans were performed on each amorphous glass sample before heat treatment or other characterization. The scans are stacked for comparison and can be seen in Figure 16. The first exothermal peak indicates the formation of hexagonal phase $BaCl_2$ and generally occurs around 240-250 ºC [32]. This peak is consistent amongst 0%-1% $FeCl_3$ samples and occurs at 243 ºC (± 3 ºC).

The second exothermal peak indicates the transformation of $BaCl_2$ nanocrystallites into the orthorhombic phase, the desired phase for application as a storage phosphor. This transformation generally occurs at 300 ºC (+/- 5 ºC) [32]. This region on each curve is indicated with a star. The 0% and 2% $FeCl_3$ samples have similar orthorhombic transformations at 300 ºC (± 8 ºC). 1% $FeCl_3$ samples, however, experience phase transformations at much cooler temperatures (278 ºC for $EuCl_2$, 283 ºC for $EuCl_3$).

A lower phase transformation temperature should result in a more translucent glass ceramic. The lower heat treatment temperature causes slower $BaCl_2$ crystal growth during the heating. By the time $BaCl_2$ has transformed into the desired orthorhombic phase, the crystals are smaller overall, leading to less occlusions and opacity in the glass ceramic. Higher heat treatment temperatures lead to larger crystals and subsequently more turbid samples. Additionally at high temperatures, partial crystallization of the glass matrix during heat treatment can cause hexagonal phase $BaCl_2$ to be consumed before its transformation to orthorhombic phase, leading to less PSL signal in the final glass ceramic [30, 33].

The DSC results determined the heat treatment temperature of samples to produce the desired phase of $BaCl_2$. A table of these temperatures is shown in Table 5.

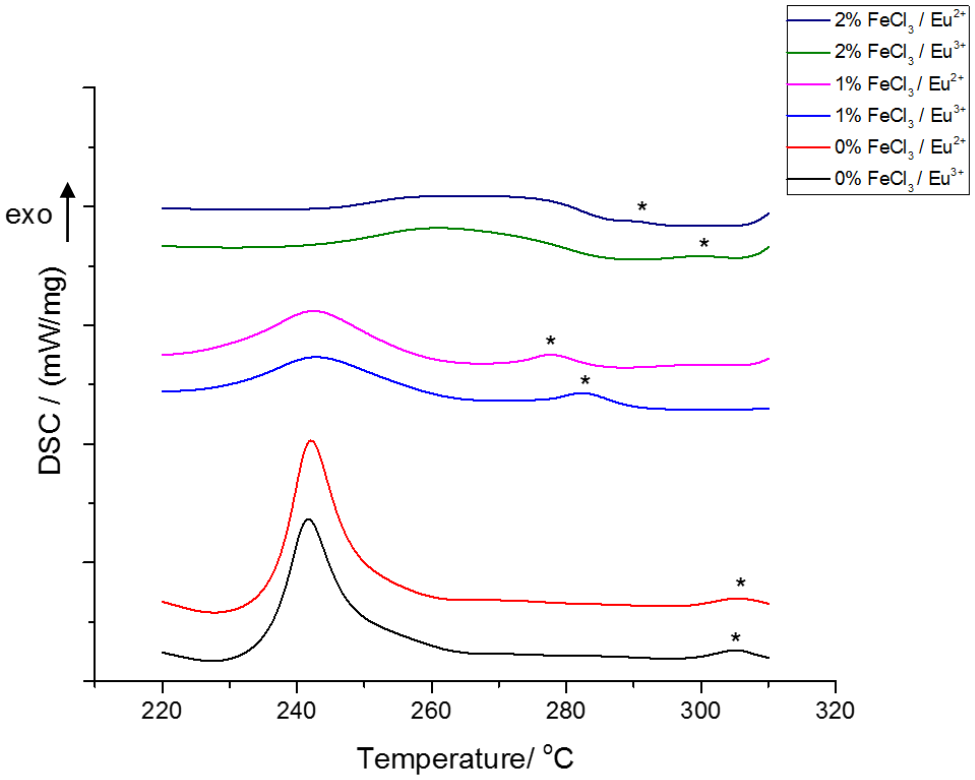

Figure 16. DSC scans results stacked for comparison. The first exothermic peak corresponds to hexagonal phase $BaCl_2$ within the FCZ matrix. Stars indicate the temperature for orthorhombic phase transformation of $BaCl_2$

Table 5. $FeCl_3$ sample heat treatment temperatures as determined by DSC scan results

Sample	Heat Treatment Temperature (ºC)
0% $FeCl_3$ / 2% Eu^{2+}	290 (hexagonal), 305 (orthorhombic)
0% $FeCl_3$ / 2% Eu^{3+}	290 (hexagonal), 305 (orthorhombic)
1% $FeCl_3$ / 2% Eu^{2+}	278
1% $FeCl_3$ / 2% Eu^{3+}	283
2% $FeCl_3$ / 2% Eu^{2+}	291
2% $FeCl_3$ / 2% Eu^{3+}	300

6. *Visual Inspection*

After heat treatment, glass ceramic samples were inspected for visual clarity/translucency. It is important for a storage phosphor to have this property; opaque samples lead to imaging artifacts and inaccuracies. Therefore, glass ceramics must be translucent if they are to be successful as imaging plates. Samples with 3% and 4% $FeCl_3$ were much too opaque to ever be successful as storage phosphor imaging plates; these samples were removed from consideration and any further characterization.

The remaining samples are shown below in Figure 17. Small pieces of each composition were placed on a paper sheet with black text. The 0% $FeCl_3$, heat treated at 290 ºC, as well as the 1% and 2% $FeCl_3$ glass ceramics were translucent enough that text could still be read through the sample. The 0% $FeCl_3$ glass ceramic, heat treated at 305 ºC, however, was completely opaque.

Glass ceramic samples were also inspected for color while exposed to 254 nm black light. This test is shown in Figure 18. As mentioned before in the Glass Ceramic Synthesis section, color can indicate what phase of $BaCl_2$ nanocrystal is present in the glass ceramic. Blue fluorescence indicates the presence of hexagonal phase nanocrystals and violet fluorescence indicates the presence of orthorhombic phase $BaCl_2$ nanocrystals within the FCZ glass matrix. A glass ceramic must have orthorhombic phase $BaCl_2$ nanocrystals if it is to be employed as a storage phosphor for medical imaging. 1% and 2% $FeCl_3$ samples exhibit the desired violet color, indicating the presence of orthorhombic phase $BaCl_2$.

After visual inspection, all 1% and 2% $FeCl_3$ samples possessed both desired properties for possible storage phosphor application: translucency and orthorhombic phase $BaCl_2$ nanocrystals. The presence of orthorhombic phase $BaCl_2$ nanocrystals was further confirmed with phosphorimetry and x-ray diffraction results in the subsequent sections.

7. *Phosphorimetry*

Phosphorimetry is able to give insight into the phase (hexagonal or orthorhombic) of $BaCl_2$ present within fluorochlorozirconate glass ceramic samples. Orthorhombic $BaCl_2$ yields an emission peak at 402 nm, while hexagonal phase $BaCl_2$ has two peaks, 410 and 470 nm. Phosphorimetry measurements were performed on the resultant glass ceramic samples. Spectra for $EuCl_2$-doped samples and $EuCl_3$-doped samples can be seen in Figure 19 and Figure 20, respectively. Both series exhibit similar phenomena. The 0% $FeCl_3$ samples at 290 ºC feature completely hexagonal crystals confirmed by their peaks at 410 nm and 470 nm. This is logical because the samples were heat treated below the required temperature for phase transformation as shown on the DSC curve (Figure 14). 0% $FeCl_3$ samples heat treated to the orthorhombic transition

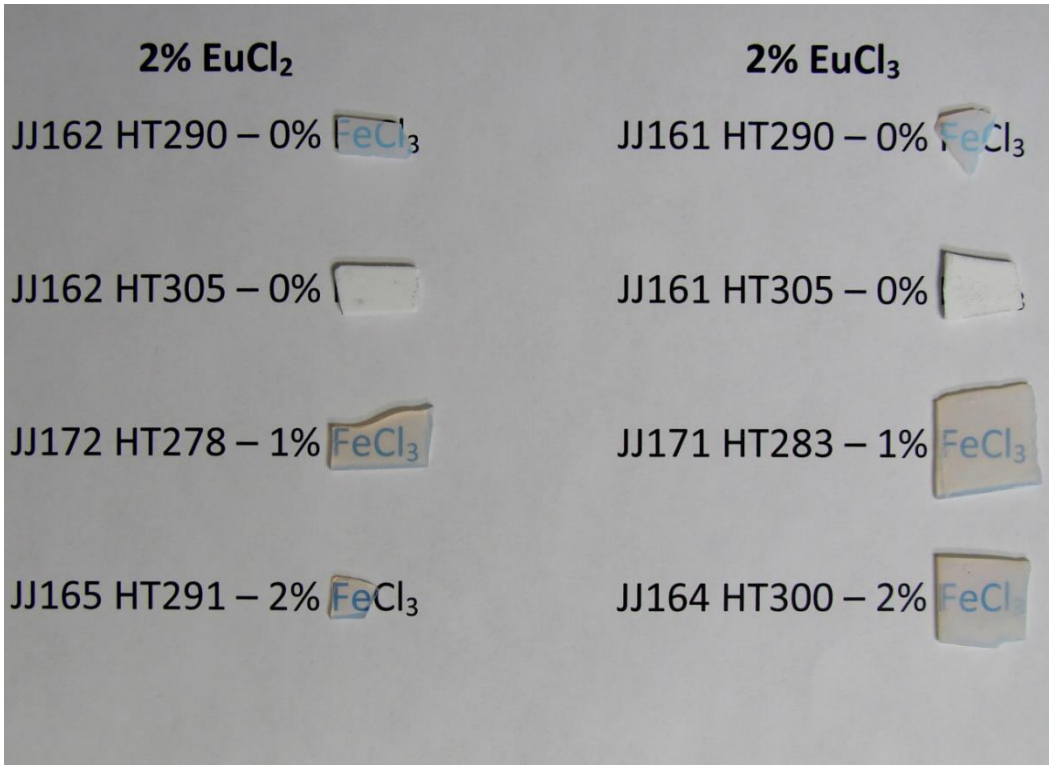

Figure 17. Visual inspection for translucency of post heat treatment samples.

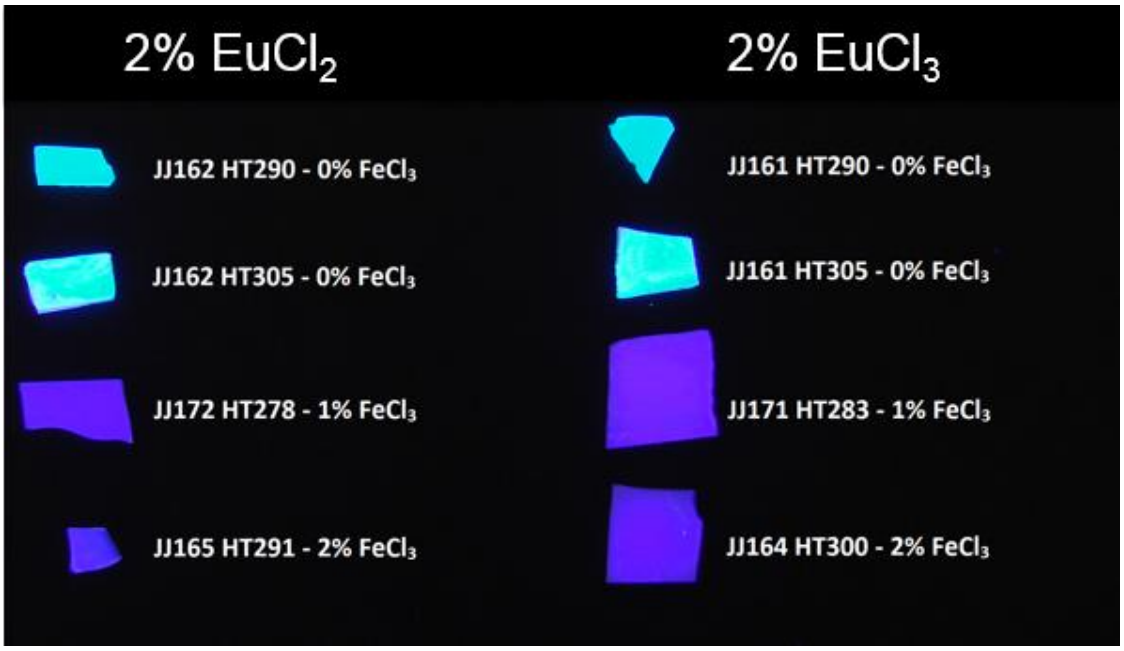

Figure 18. Samples exposed to 254 nm black light post heat treatment for $BaCl_2$ phase inspection. Blue/cyan corresponds to hexagonal phase $BaCl_2$ nanocrystals, while violet corresponds to orthorhombic phase $BaCl_2$:Eu^{2+} nanocrystals within the FCZ glass matrix.

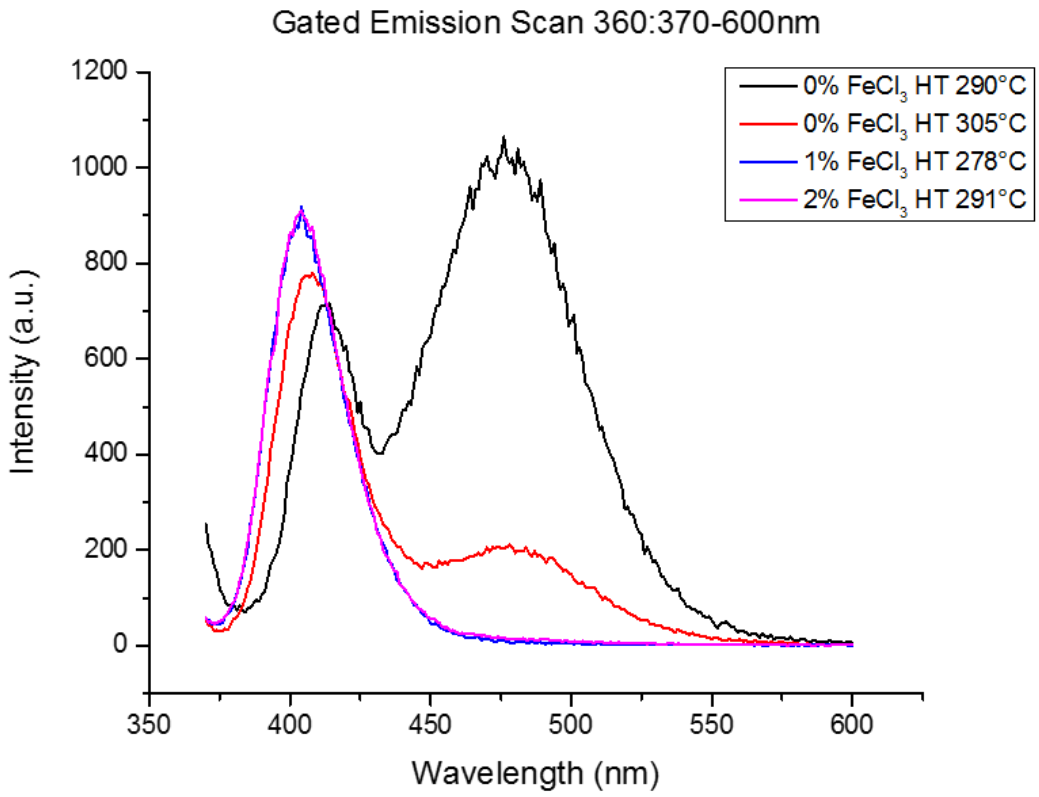

Figure 19. PL emission spectra where $EuCl_2$ samples were excited at 360 nm and observed between 370 and 600 nm

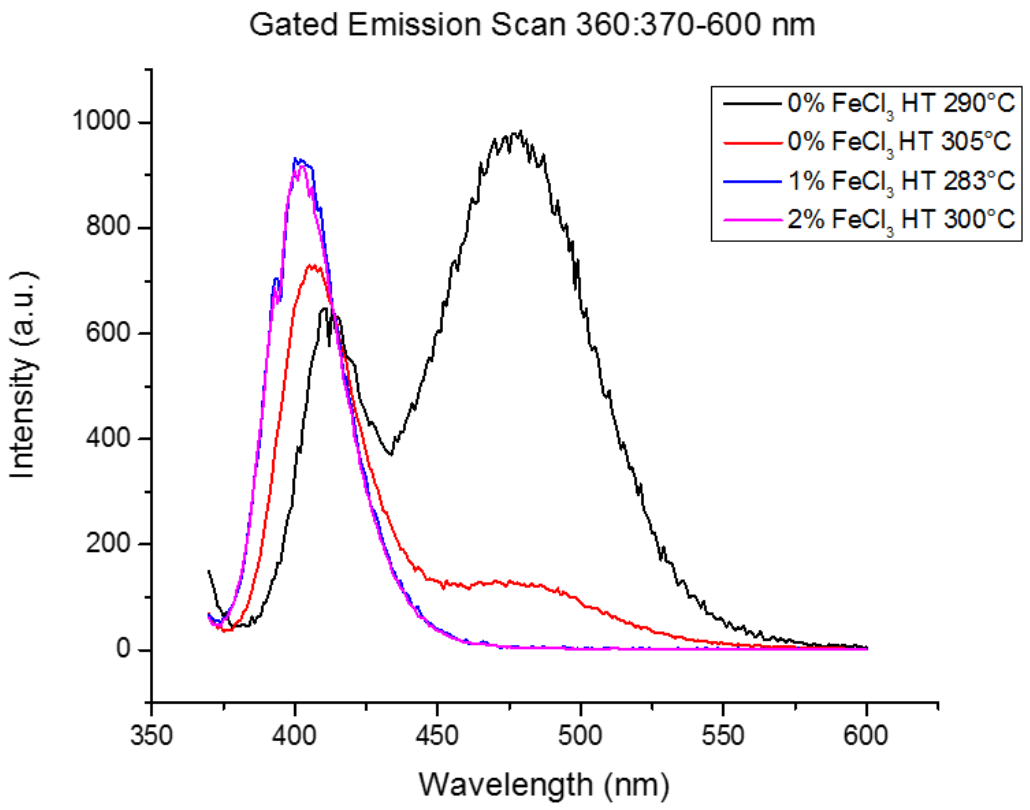

Figure 20. PL emission spectra where $EuCl_3$ samples were excited at 360 nm and observed between 370 and 600 nm

temperature shown on the DSC curve (305 ºC) only exhibit partial transformation in the PL spectra. The peak at 470 nm shrinks in intensity but does not entirely disappear. The 410 nm peak experiences a partial shift to 406 nm, further implying the existence of both $BaCl_2$ hexagonal and orthorhombic phases within the glass ceramic. This partial transformation is attributed to the high temperature of heat treatment; some $BaCl_2$ crystals grew to too large of a size before transforming into the orthorhombic phase. The large crystals also contribute to the sample's opacity.

The spectra for 1% and 2% $FeCl_3$ samples show a single peak at 402 nm, indicting the presence of solely orthorhombic $BaCl_2$. Phosphorimetry results confirm that the inclusion of small amounts of $FeCl_3$ within the FCZ glass composition allows for the orthorhombic phase transformation of $BaCl_2$ to occur at lower temperatures.

8. X-Ray Diffraction (XRD)

X-ray diffraction scans are stacked for comparison in Figure 21. XRD peaks are used to identify the phases of $BaCl_2$ in the sample. The orthorhombic phase $BaCl_2$ powder diffraction file (PDF # 24-0094) is superimposed on the bottom of the graph. The peaks of the 1% and 2% $FeCl_3$ samples match those of the reference file, indicating the presence of orthorhombic phase $BaCl_2$ nanocrystals in the samples.

9. Photostimulated Luminescence (PSL)

After characterization at UTSI, glass ceramic samples were sent to SUNY Stony Brook for photostimulated luminescence experiments to measure their integrated PSL signal. This is analogous to the total PSL light output of the sample. Results of PSL experiments can be seen in Figure 22. Light output is correlated with opacity of the sample. Higher light outputs are desired for storage phosphor applications. However, opaque samples are not desired because of inaccuracies in imaging. A balance must be struck between light output and opacity of the sample.

The three samples with the highest PSL signal were 0% $FeCl_3$ / 2% $EuCl_3$,1% $FeCl_3$ / 2% $EuCl_3$, and 2% $FeCl_3$ / 2% $EuCl_3$. The 0% $FeCl_3$ sample, however, was completely opaque upon visual inspection, making it a poor candidate for accurate storage phosphor imaging. Therefore, the 1% $FeCl_3$ / 2% $EuCl_3$ and 2% $FeCl_3$ / 2% $EuCl_3$ glass ceramic samples were the best candidates for imaging when accounting for translucency and light output.

Interestingly, all samples doped with $EuCl_3$ exhibited much greater PSL signal when compared to their $EuCl_2$ counterparts. A possible explanation for this

phenomenon is evaporation during the melt in the furnace. Chlorides have been known to evaporate while exposed to high temperatures in the furnace during synthesis [13]. This results in an amorphous glass with less chlorine content overall. Less chlorine content leads to less $BaCl_2$:Eu^{2+} coordination upon heat treatment, which subsequently results in a lower luminescence output. By doping with $EuCl_3$ instead of $EuCl_2$, significantly more chlorine ions are added to the composition and survive the evaporation losses of the melt, leading to more $BaCl_2$:Eu^{2+} coordination and a higher light output.

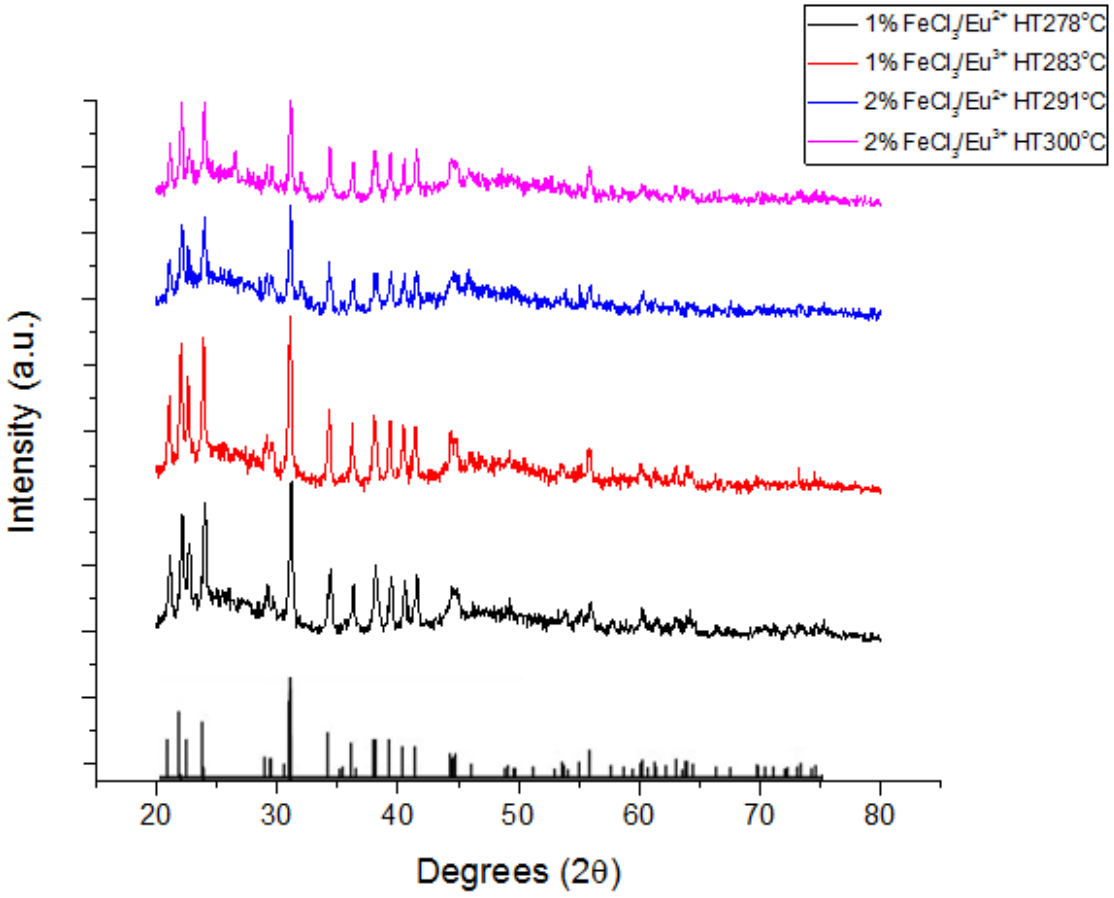

Figure 21. X-ray diffraction scans for 1% and 2% $FeCl_3$ glass ceramics to confirm the presence of orthrorhomibc phase $BaCl_2$ nanocrystals. The orthorhombic phase $BaCl_2$ powder diffraction file (PDF # 24-0094) is superimposed on the bottom of the graph for comparison.

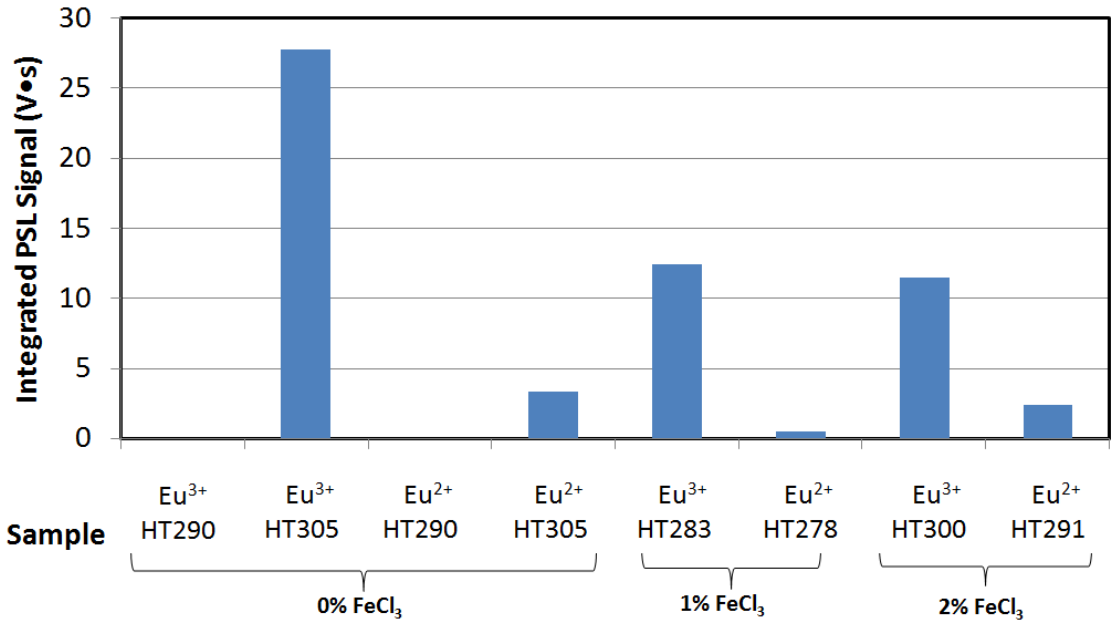

Figure 22. Integrated photostimulated luminescence signal of glass ceramic sample with 0-2% $FeCl_3$

Glass Ceramic Imaging Plates

10. Differential Scanning Calorimetry (DSC)

DSC scans were performed on each amorphous glass plate before heat treatment or other characterization. The heating rate for ZBLAN30 was 1 ºC per minute, while ZBLAN40 was heated at 5 ºC per minute. ZBLAN40 was heated more quickly in an attempt to make the orthorhombic peak more discernable. The scans are stacked for comparison and can be seen in Figure 23. The first exothermal peak indicates the formation of hexagonal phase $BaCl_2$. This peak occurs at 225 ºC for ZBLAN30 and 265 ºC for ZBLAN40.

The second exothermal peak indicates the transformation of $BaCl_2$ nanocrystallites into the orthorhombic phase, the desired phase for application as a storage phosphor. This region on each curve is indicated with a star. ZBLAN30 experiences this change at 275 ºC, while ZBLAN40 transforms at 305 ºC.

The DSC results determined the heat treatment temperature of samples to produce the desired phase of $BaCl_2$.

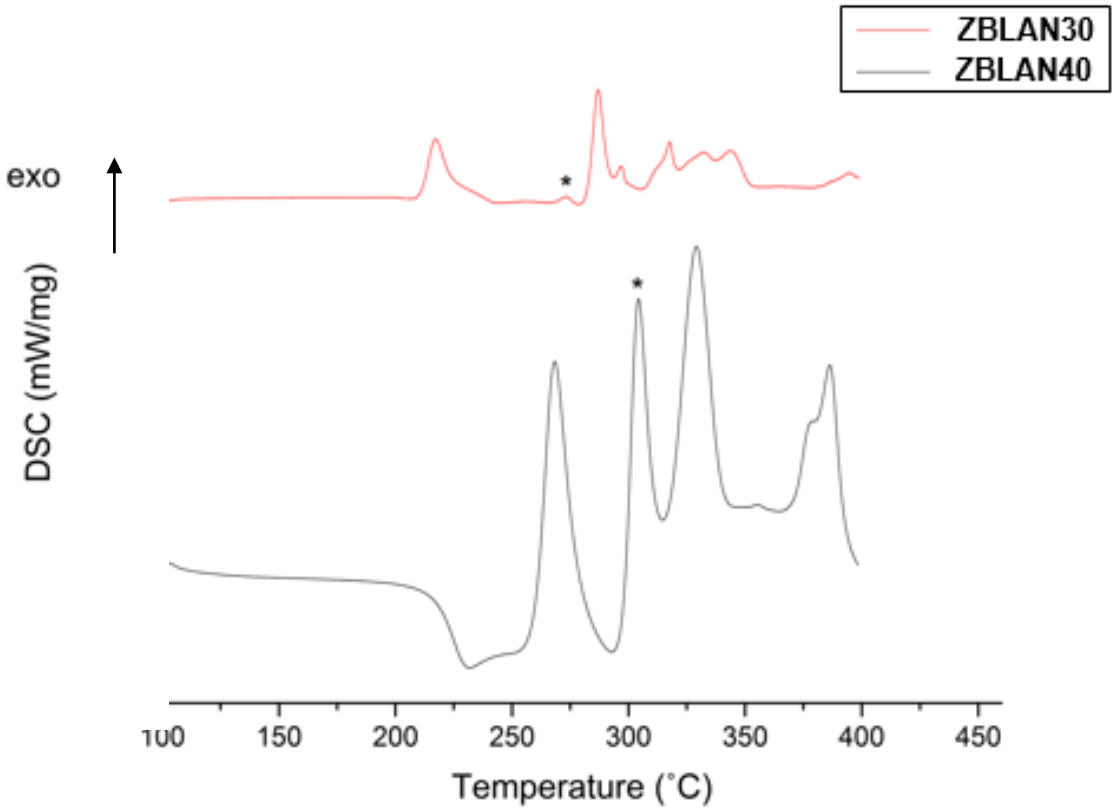

Figure 23. Imaging plate DSC scans results stacked for comparison. The first exothermic peak corresponds to hexagonal phase $BaCl_2$ within the FCZ matrix. Stars indicate the temperature for orthorhombic phase transformation of $BaCl_2$. The heating rate for ZBLAN30 was 1 ºC/min, while the heating rate for ZBLAN40 was 5 ºC/min.

11. Computed Radiography Images

After heat treatment into glass ceramics, imaging plates were exposed at energies of 45 keV, 70 keV, 300 keV, and 1 MeV. A variety of subjects were imaged, including a European hornet, socket head cap screw, weld phantom, and gap phantom. The variety of materials, from the soft biomass of the hornet to the metal of the various phantoms, allows for the capability of plates to be tested over a wide range.

An image of a European hornet is shown in Figure 24. Exposed at 45 keV on ZBLAN30, the separate anatomical features of the hornet are able to be distinguished, including the antennae, head, thorax, and abdomen.

A socket head cap screw was imaged at 1 MeV with ZBLAN40, and the resultant image is shown in Figure 25. All the features of the socket head cap screw (threads, head, and socket) are able to be distinguished.

A weld phantom was imaged at 1 MeV, and a picture of the phantom is shown in Figure 26. A weld phantom contains a weld with a known defect or inconsistency. Knowing where the inconsistency is located allows for the phantom to act as a test of image resolution. A computed radiography image of the weld phantom on ZBLAN30 is shown in Figure 27. The defect is seen in both the original image and the blown-up cutaway, meaning the scanner and plate were able to achieve adequate resolution for this application.

A gap phantom was imaged at 1 MeV, and a picture of the phantom is shown in Figure 28. A gap phantom consists of separations, or "gaps," of known thicknesses within the metal block. Knowing the size of the gaps allows for the phantom to act as a test for the limits of crack detection. A computed radiography image of the gap phantom on ZBLAN40 is shown in Figure 29. All of the different sized gaps were able to be distinguished. Thicker gaps appeared larger/darker on the computer radiography image.

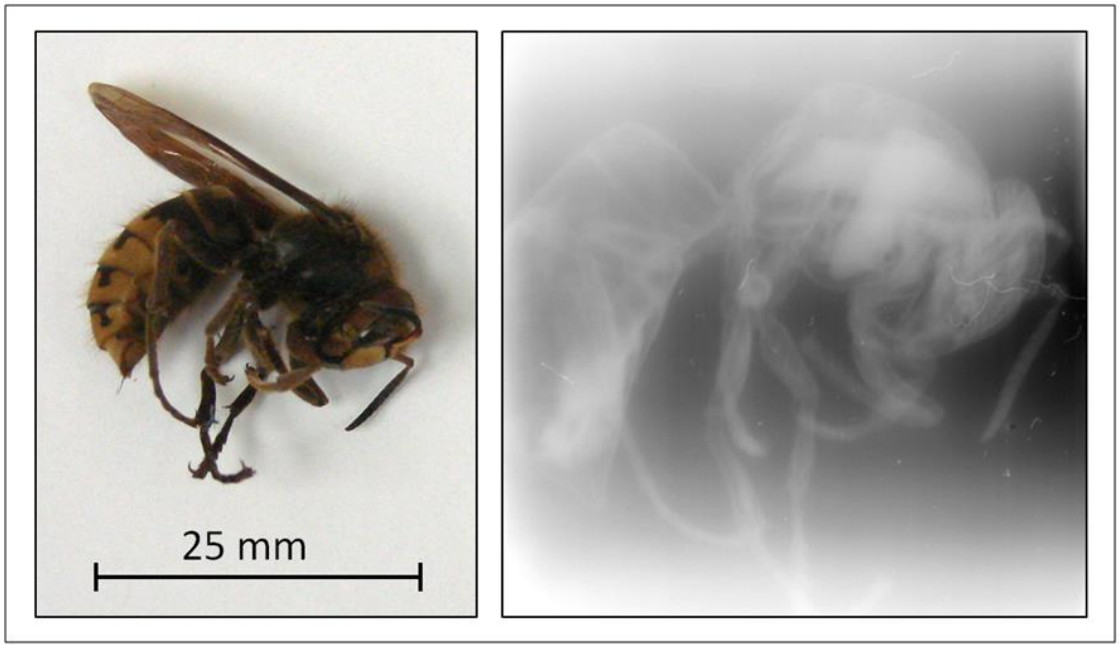

Figure 24. CR image of a European hornet exposed at 45 keV.

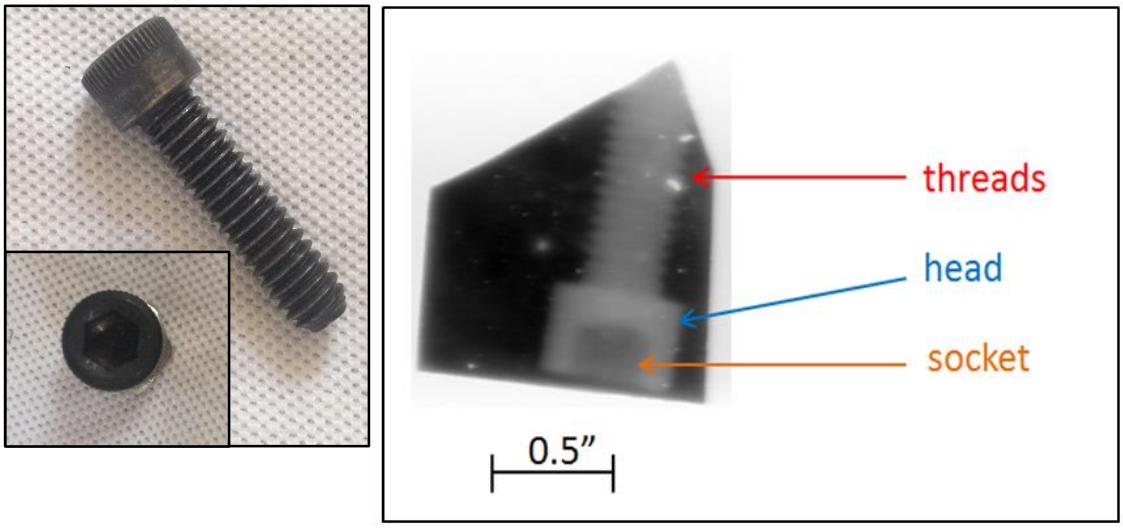

Figure 25. CR image of a socket heat cap screw exposed at 1 MeV.

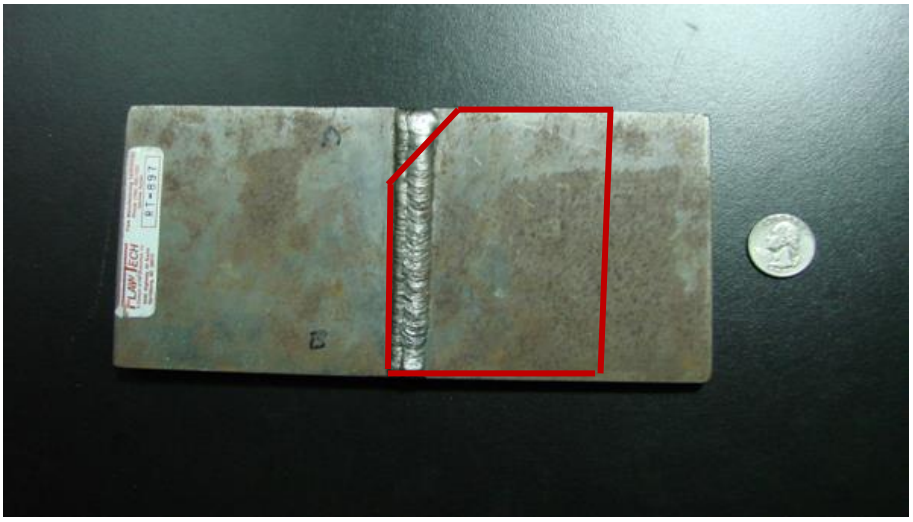

Figure 26. Weld phantom used for CR image testing. Quarter included for scale. The outline indicated where the ZBLAN30 plate was placed behind the weld phantom.

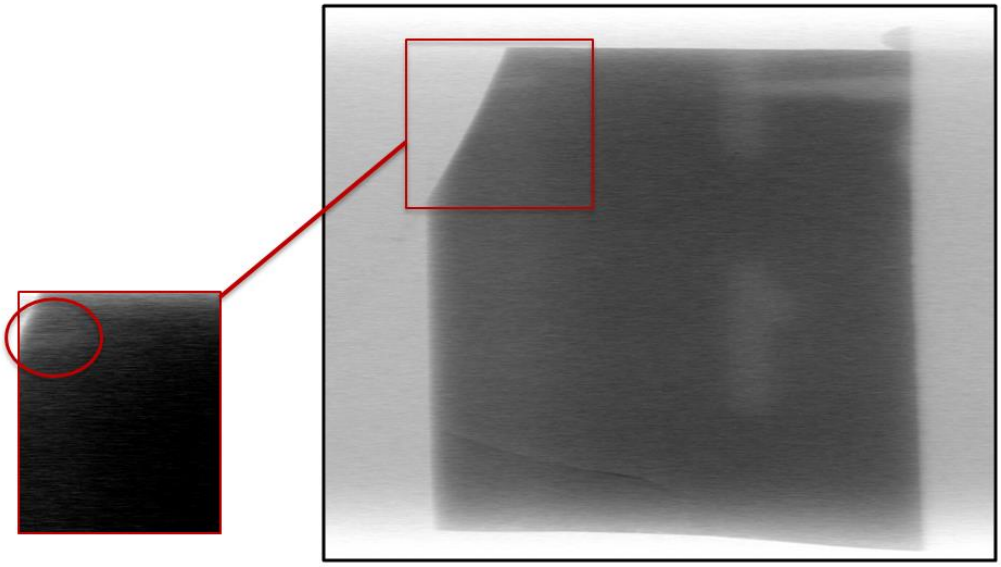

Figure 27. CR image of weld phantom exposed at 1 MeV. Inconsistency in weld (lighter region in blown up section) was able to be detected.

Figure 28. Gap phantom used for CR image testing [30]. Used with permission.

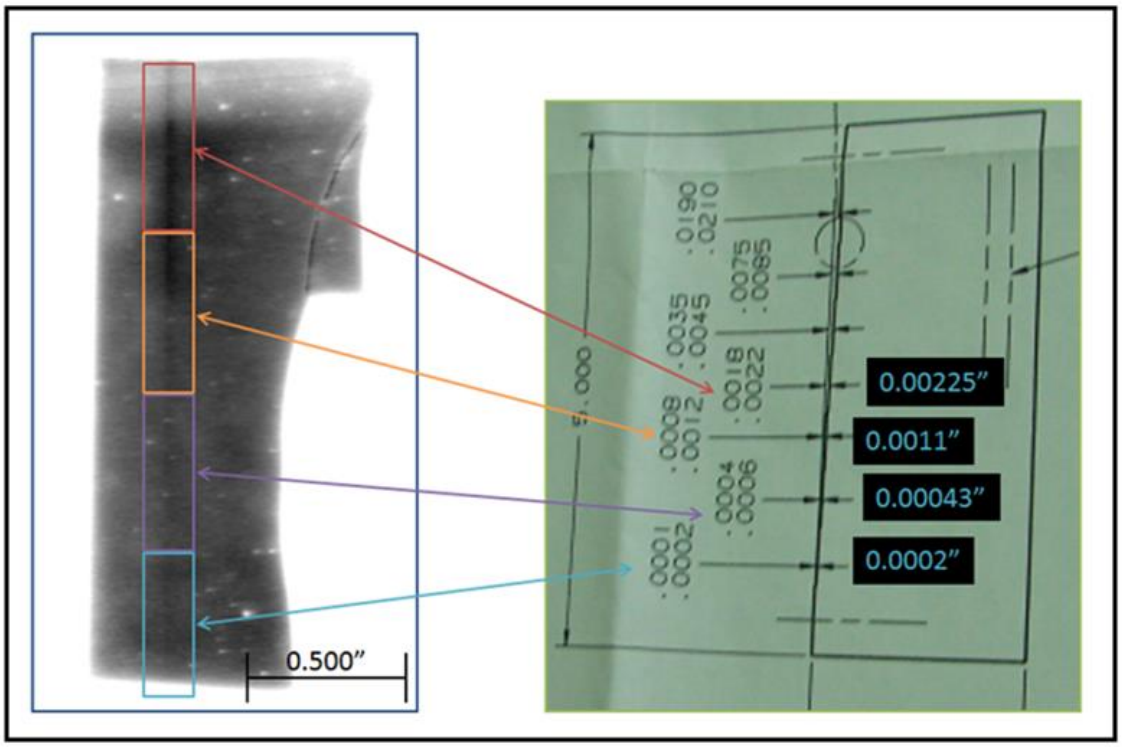

Figure 29. CR image of gap phantom exposed at 1 MeV. Larger gaps appear as thicker/darker lines in the CR image.

12. Plot Profiles/ Line Pair Phantoms

In image processing, a line pair is a test pattern consisting of regularly spaced black and white parallel lines. A line pair phantom is a metal sheet with the line pair test pattern cut into the material. Figure 15 shows an example of a line pair phantom. The phantom can be placed on the imaging plate and used as a measure of spatial resolution.

A line pair phantom was imaged at 45 keV on ZBLAN30. The resulting image is shown in Figure 30. A plot profile of the image was taken in the imaging software ImageJ and also shown in the figure. Each valley in the plot profile corresponds to a separation between line pairs. Since the phantom contains five line pairs, five valleys mean that the scanner/plate is able to resolve the separation at the given resolution on line pair phantom's scale. Using this plot profile tool, a spatial resolution of at least 20 line pairs per millimeter was determined for ZBLAN30 at 45 keV. This measurement was at the line pair phantom’s limit.

The same line pair phantom was imaged at 70 keV on ZBLAN40. The resultant computed radiography image is shown in Figure 31. Using the same plot profile method, a spatial resolution of 4.5 line pairs per millimeter was determined.

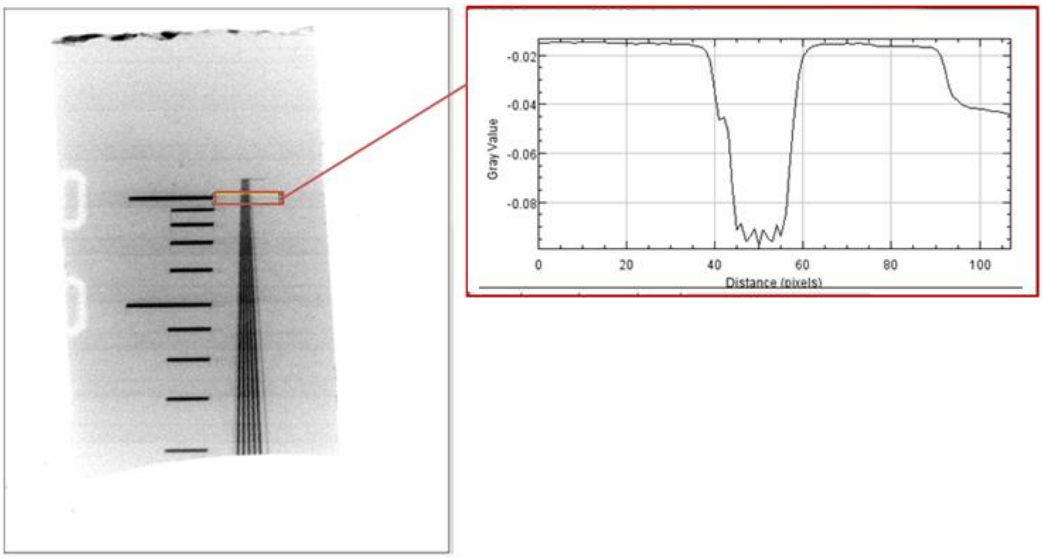

Figure 30. CR image of line pair phantom exposed at 45 keV with adjacent plot profile. Resolution was determined to be 20 line pairs per millimeter.

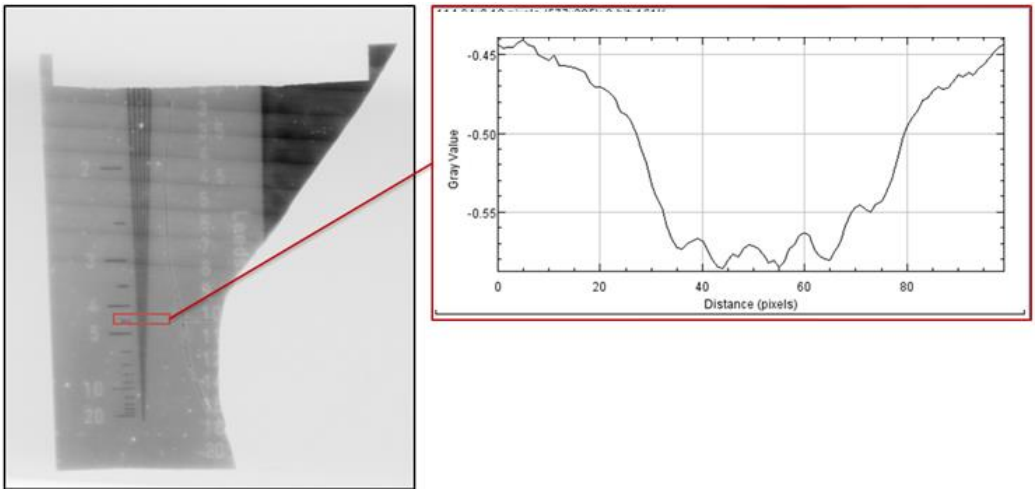

Figure 31. CR image of line pair phantom exposed at 70 keV with adjacent plot profile. Resolution was determined to be 4.5 line pairs per millimeter.

These images demonstrate a trend of decreasing resolution and overall image quality with increasing x-ray energy. At higher energies, Compton scattering (inelastic scattering of a photon by a charged particle) is dominant over photoelectric absorption. This scattering can cause loss of resolution. Also, as x-ray energy increases, a higher percentage of radiation will pass through both the subject and the storage phosphor without interaction, reducing image contrast.

13. Modulated Transfer Function Calculations

Computed radiography images were also made of edge phantoms at 45 keV and 300 keV. Edge phantoms are a metal sheet that defines a sharp difference, or "edge," between an attenuated and nonattenuated region of the imaging plate.

Computed radiography images at 45 keV of an edge phantom with ZBLAN30 and the same edge phantom with a GE IPU commercial plate are shown in Figure 32. Resultant modulation transfer function calculations are shown in Figure 33. From Figure 32, the GE IPU plate has a much higher spatial resolution when compared to ZBLAN30. This result is clearly seen in the comparison of the CR images. ZBLAN30's edge is slightly occluded, while the commercial plate's edge is sharp and well defined.

A computed radiography image of an edge phantom with ZBLAN30 at 300 keV is shown in Figure 34 with an accompanying modulation transfer function generation in Figure 35. The modulation transfer function (MTF) is a measurement of an imaging system’s ability to transfer contrast at a certain resolution from an object to the resulting image, combining resolution and contrast into a single quantity [34]. As spatial resolution increases, it becomes more difficult for the imaging system to transfer the decrease in contrast to the image, and MTF subsequently decreases.

ZBLAN30 had low resolution at 300 keV. A stacked plot of MTF's at 45 keV and 300 keV for comparison is shown in Figure 36. Both images had low resolution as determined by modulation transfer function, but a trend of resolution decreasing as energy increases can be seen. As with the line pair phantoms, this can be attributed to increased Compton scattering and decreased attenuation in both the subject being imaged and the storage phosphor due to higher x-ray energies.

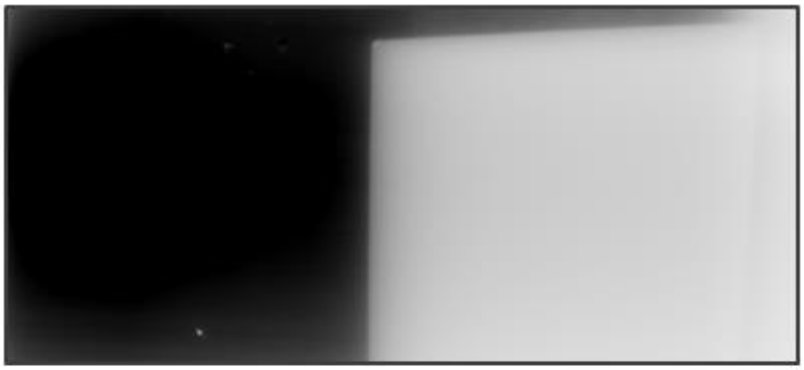

ZBLAN30 Glass Ceramic Plate

General Electric IPU Plate

Figure 32. Cutaway CR images of edge phantoms exposed at 45 keV on sample and commercial plates.

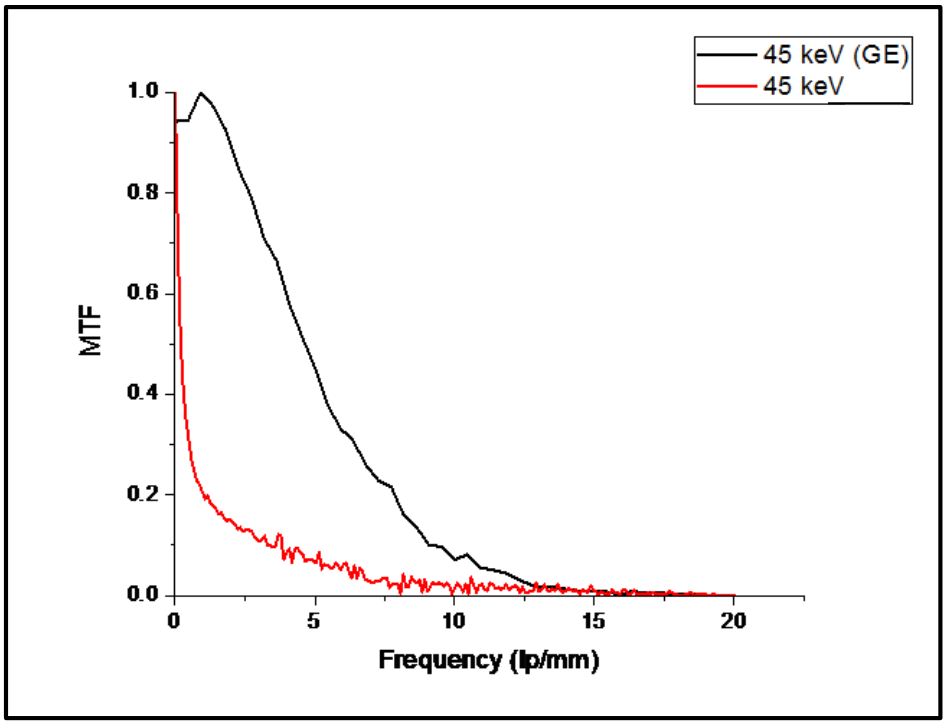

Figure 33. Modulation transfer function results generated for edge phantoms exposed at 45 keV on a commercial plate and ZBLAN30 plate.

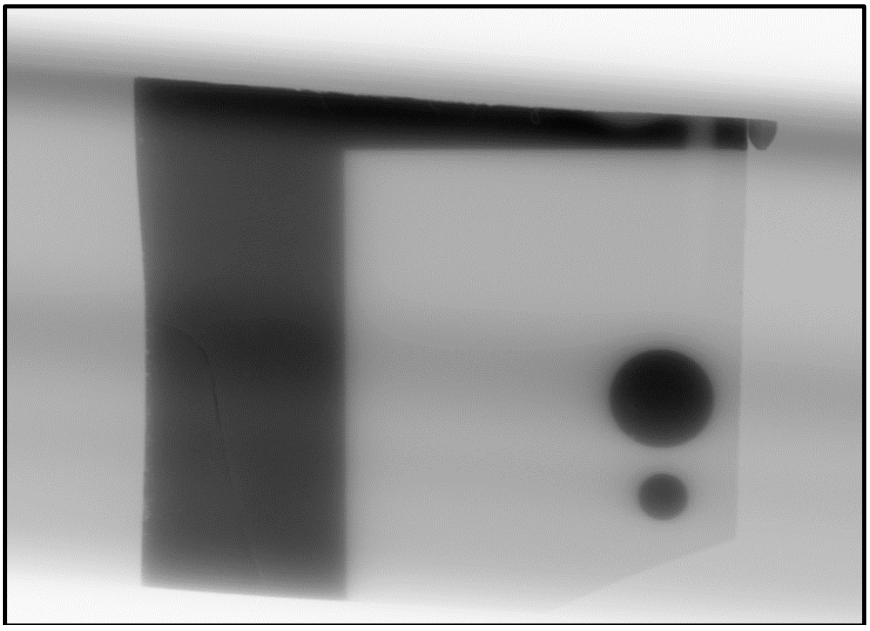

Figure 34. CR image of an edge phantom exposed at 300 keV on a sample plate.

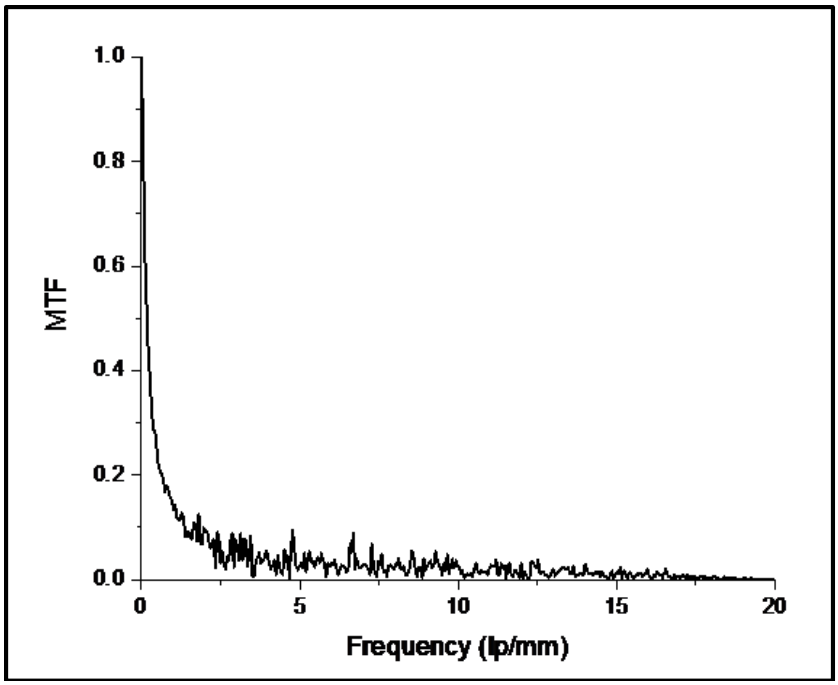

Figure 35. Resultant modulation transfer function for edge phantom exposed at 300 keV with ZBLAN30 plate.

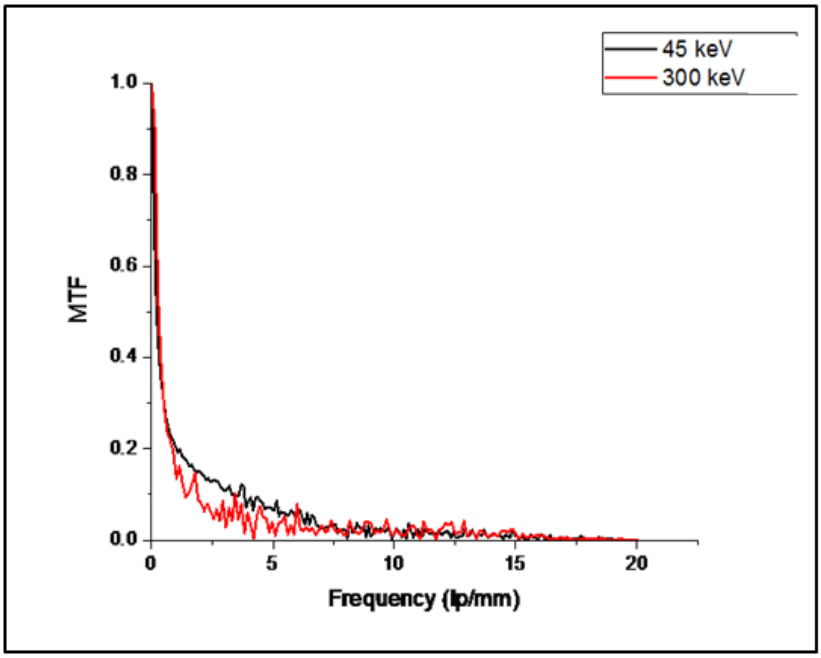

Figure 36. Comparison of MTF results for edge phantoms exposed at 45 keV and 300 keV with ZBLAN30 plate. Lower energy edge phantom images had higher spatial resolution and less noise.

CHAPTER 4:

CONCLUSIONS

The addition of small amounts of $FeCl_3$ (1-2%) to a ZBLAN glass composition allows for the precipitation of orthorhombic phase $BaCl_2$ crystals while maintaining transparency of the glass-ceramic. This occurs because $FeCl_3$ lowers the orthorhombic phase transition indicated on the DSC curve. Increased chlorine content from the addition of $FeCl_3$ allows $BaCl_2$ crystallites to form and transform more quickly during heat treatment. A lower phase transition temperature leads to smaller $BaCl_2$ crystallites in the matrix. Smaller crystallites not only result in a more transparent sample, but also less internal scattering within the sample during photostimulated luminescence. Less internal scattering leads to higher resolution images. Overall, the 1% $FeCl_3$, 2% $EuCl_3$ sample heat treated at 283 ºC offered the best combination of light output and sample transparency.

Future work on $FeCl_3$ samples should include spectrophotometry experiments to objectively measure the amount of translucency in the glass ceramic. A series without the stabilizer InF_3 could be synthesized to investigate the effect Fe^{3+} has on the stability on the glass matrix. Additionally, a series replacing $FeCl_3$ with FeF_3 could be made to separate the effect of Fe^{3+} from chlorine on light output/PSL.

FCZ glass ceramic storage phosphors were synthesized for usage as an imaging plate for computed radiography at various x-ray energies. After imaging various phantoms and everyday items, the feasibility of FCZ glass ceramics containing $BaCl_2$:Eu^{2+} was confirmed for this application as an imaging material. In the future, commercial plates should be tested and imaged at higher energies for a comparison to FCZ samples. Additionally, FCZ plates should be synthesized at larger thicknesses to determine their ability to image at higher x-ray energies with larger penetration power.

REFERENCES

1. Poulain, M., M. Poulain, and J. Lucas, Verresfluores au tetrafluorure de zirconium proprieties optiques d'un verre dope au ND3+.Materials Research Bulletin, 1974.10(4): p. 243-246.

2. Poulain, M. and A. Soufiane, Fluoride Glasses: Synthesis and Properties.Brazilian Journal of Physics 1992.22(3): p. 205-217.

3. Fedorov, V., A. Babitsyna, and T. Emel'yanova, Glass Formation in the ZrF4-LaF3-BaF2-NaF System.Glass Physics and Chemistry 2001.27(6): p. 512-519.

4. Brekhovskikh, M. N., et al. (2009). "Glasses Based on Fluorides of Metals of the I-IV Groups: Synthesis, Properties, and Application." Inorganic Materials 45(13): 1477-1493.

5. McNamara, P. and R. H. Mair (2005). "Devitrification Theory and Glass-Forming Phase Diagrams of Fluoride Compositions" Micro- and Nanotechnology: Materials, Processes, Packaging, and Systems II, Bellingham, WA, Proceedings of SPIE.

6. Zhu, X. and N. Peyghambarian, High-Power ZBLAN Glass Fiber Lasers: Review and Prospect.Advances in OptoElectronics, 2010.2010: p. 23.

7. Schweizer, S., et al. (2010). "Multi-functionality of fluorescent nanocrystals in glass ceramics." Radiation Measurements45: 4850489.

8. Seggern, H. v. (1999). "Photostimulable X-Ray Storage Phosphors: a Review of Present Understanding." Brazilian Journal of Physics 29(2): 254-268.

9. Schewizer, S. (2001). "Physics and Current Understanding of X-Ray Storage Phosphors." Physica Status Solidi A 187(2): 335-393.

10. Alvarez, C. J., et al. (2013). "Nanocrystallization in Fluorochlorozirconate Glass-Ceramics" Journal of the American Ceramic Society 96(11): 3617-3621.

11. Johnson, J. A., et al. (2007). "A Glass-Ceramic Plate for Mammography." Journal of the American Ceramic Society 90(3): 693-698.

12. Edgar, A., et al., A new fluorozirconate glass-ceramic X-ray storage phosphor.Journal of Non-Crystalline Solids, 2003.326: p. 489-493.

13. Chen, G., et al., Insights into phase formation in fluorochlorozirconate glass-ceramic storage phosphors. Applied Physics Letters, 2006.88(191915).

14. Johnson, J., et al., Crystallization in heat-treated fluorochlorozirconate glasses. Journal of Physics: Condensed Matter, 2009. 21.

15. Johnson, J. A., et al. (2015). "Opportunities for Fluorochlorozirconate and Other Glass-Ceramic Detectors in Medical Imaging Devices." Journal of Biomedical Technology and Research 1(1): 102.

16. Schweizer, S., et al. (2002). "Development of X-Ray Storage Phosphor Glass-Ceramics." Radiation Effects & Defects in Solids: Incorporating Plasma Science and Plasma Technology 157(6-12): 895-902.

17. Leonard, R. L., et al. (2013). "Rare earth doped downshifting glass ceramics for photovoltaic applications." Journal of Non-Crystalline Solids 366: 5.

18. Paßlick, C., et al., Differential scanning calorimetry investigations on Eudopedfluorozirconate-based glass ceramics.Journal of Non-Crystalline Solids, 2010.356: p. 3085-3089.

19. Pfau, C., et al., Phonon spectra of barium halide nanocrystals in fluorozirconate glasses. IOP Conf. Series: Materials Science and Engineering, 2010. 15(012021).

20. Paßlick, C., et al., Structural properties of fluorozirconate-based glass ceramics doped with multivalent europium.Journal of Applied Physics, 2011.110.

21. Leonard, R. L., et al. (2015). "Evaluation of a Fluorochlorozirconate Glass-Ceramic Storage Phosphor Plate for Gamma-Ray Computed Radiography." Journal of the American Ceramic Society: 7.

22. Alvarez, C. J., et al. (2015). "Structural and Kinetic Analysis of BaCl2 Nanocrystals in Fluorochlorozirconate Glass-Ceramics." Journal of the American Ceramic Society 98(4): 1099-1104

23. Schweizer, S., et al. (2005). "Photostimulable defects in nano-crystallites in fluorozirconate glasses." Physica Status Solidi A202(2): 243-249.

24. Edgar, A., et al. (2004). Optical properties of a high-efficiency glass ceramic x-ray storage phosphor. Radiation Measurements, 38, 413-416.

25. Leblans, P., et al. (2011). "Storage Phosphors for Medical Imaging." Materials4: 1034-1086

26. Schweizer, S., et al. (2007). “Fluorozirconate-based glass-ceramic storage phosphors for digital mammography.” Medical Imaging 2007: Physics of Medical Imaging.

27. Mathew, J. and R. Doremus (1988). "Vaporization of zirconium fluoride glasses." Journal of Non-Crystalline Solids: 165-172.

28. Secu, M., et al. (2003). "Phototstimulated luminescence from a flurobromozirconate glass-ceramic and the effect of crystallite size and phase." Journal of Physics: Condensed Matter 15: 1097-1108.

29. Rowlands, J.A. (2002). "The physics of computed radiography." Physics in Medicine and Biology. 47: R123-R166.

30. Leonard, Russell Lee, "Fluorochlorozirconate Glass Ceramics for Photovoltaic and Computed Radiography Applications." PhD diss., University of Tennessee, 2015. http://trace.tennessee.edu/utk_graddiss/3505

31. Lubinsky, A.R. (2012). "Scanning translucent glass-ceramic x-ray storage phosphors." Proc SPIE. 2010; 7622: 76223W.doi: 10.1117/12.843346

32. King, J.E. (2015). “Doping of fluorochlorozirconate and borate-silica glass ceramics for medical imaging and fast neutron scintillation.” Master’s Thesis, University of Tennessee, 2015. http://trace.tennessee.edu/utk_gradthes/3414

33. Alvarez, C.J. (2015). “Crystallization kinetics in fluorochloroziroconate glass-ceramics.” Doctoral Dissertation. Retrieved from ProQuest (3705208)

34. Perry, Brian, "Algorithm for MTF estimation by histogram modeling of an edge" (2001). Thesis. Rochester Institute of Technology. Accessed from http://scholarworks.rit.edu/theses/6788

VITA

Adam Wesley Evans was born in Knoxville, Tennessee on June 30, 1990. He was raised in Knoxville, Tennessee and graduated from Bearden High School in 2009. He graduated from The University of Tennessee, Knoxville with a Bachelor of Science Degree in Biomedical Engineering in 2013. After a gap year, he returned to the University of Tennessee system in 2014, this time at The University of Tennessee Space Institute to pursue a Master's Degree in Biomedical Engineering.